UQAC
Université du Québec
à Chicoutimi

PRECIPITATION BEHAVIORS OF DISPERSOIDS INDUCED FROM TRANSITION ELEMENTS (Mn, Sc AND Zr) AND THEIR EFFECT ON RECRYSTALLIZATION RESISTANCE IN AA6082 ALLOYS

Par

Chen Li

MÉMOIRE PRÉSENTÉE À L'UNIVERSITÉ DU QUÉBEC À CHICOUTIMI EN VUE DE L'OBTENTION DU GRADE DE MAÎTRISE EN INGÉNIERIE

Québec, Canada

RÉSUMÉ

Pour satisfaire la demande croissante d'alliages d'aluminium appliqué à haute température ou transformé en forme souhaitée sans sacrifier la résistance mécanique, l'amélioration des propriétés à température élevée et de la résistance à la recristallisation lors de la déformation à chaud et le recuit est très importante. Le présent travail a atteint les deux objectifs en introduisant des dispersoïdes en ajoutant des éléments de transition, tels que Mn, Zr et Sc. Bien que de nombreux travaux aient été réalisés sur ce sujet, plusieurs aspects doivent encore être clarifiés, à savoir les effets des éléments de transition et leur interaction, ainsi que les traitements thermiques. Par conséquent, dans ce projet, Mn, Zr et Sc ont été ajoutés aux alliages Al-Mg-Si 6082 pour effectuer les recherches.

Comme première étape, le comportement en précipitation de dispersoïdes contenant du Mn dans un alliage Al-Mg-Si 6082 avec différentes teneurs en Mn (jusqu'à 1% en poids) au cours de différentes procédures de traitement thermique (300-500 ℃) a été systématiquement étudié. Parallèlement, le rôle des dispersoïdes sur la résistance à température élevée et la résistance à la recristallisation lors du laminage à chaud et du recuit a été traité. Les résultats ont montré que, quelle que soit la teneur en Mn, les dispersoïdes ont commencé à précipiter à 350 ℃ et ont atteint à la condition optimale au bout de 2 heures à 400 ℃, conduisant à la microdureté la plus élevée à la température ambiante et à la limite d'élasticité à 300 ℃. Cependant, les dispersoïdes

grossissent progressivement à des températures supérieures à 450 ℃. L'augmentation de Mn de 0.5 à 1.0% augmente généralement la densité en nombre des dispersoïdes mais l'évolution de la taille est fortement liée à la température. C'est similaire avec les alliages avec les teneurs en Mn de 0.5 et 1.0% à basse température (<= 400 ℃), tandis que le taux de grossissement du dispersoïde dans l'alliage à 1.0% Mn est beaucoup plus élevé à une température plus élevée (>450 ℃). Pendant le recuit après laminage à chaud, la présence de dispersoïdes contenant du Mn a considérablement amélioré la résistance à la recristallisation, bien que le volume de recristallisation augmente avec le temps de recuit dans tous les alliages expérimentaux. De plus, la résistance supérieure à la recristallisation a été obtenue dans l'alliage contenant 0.5% de Mn (par rapport à l'alliage de 1.0% de Mn), qui a été attribué à son taux plus rapide de grossissement des particules de dispersion pendant le recuit et la taille de grain d'origine plus grande avant le laminage.

D'après les résultats obtenus ci-dessus, Des éléments Zr et Sc ont également été ajoutés à l'alliage contenant 1.0% de Mn, afin d'étudier l'effet de l'addition de Zr et de Sc sur les dispersoïdes contenant du Mn dans diverses conditions de traitement thermique et d'interactions entre Al_3Zr, $Al_3(Sc,Zr)$ et des dispersoïdes contenant du Mn. On a constaté que l'addition individuelle de Zr et l'addition combinée de Sc et de Zr avaient des influences différentes sur les dispersoïdes contenant du Mn en fonction de la température de traitement thermique. À 350 ℃, l'addition combinée de Zr et de Sc a significativement supprimé la précipitation de dispersoïde contenant du Mn,

lorsque l'effet de l'addition individuelle de Zr était moins important. À 400 ℃, l'addition individuelle de Zr a inhibé la précipitation de dispersoïde contenant du Mn mais un effet négligeable a été observé avec les additions combinées de Zr et de Sc. À 450 ℃, pourtant, les dispersoïdes contenant du Mn n'étaient plus supprimés dans les deux cas. Le mécanisme à l'origine de tels phénomènes a été attribué à la nucléation préférentielle du dispersoïde d'Al_3Zr en phase u et alors la consommation simultanée de la phase u, empêchant ainsi la précipitation du dispersoïde contenant du Mn, qui préfère également se nucléer en phase u. la même raison devait s'appliquer au dispersoïde d'$Al_3(Sc,Zr)$, puisque les dispersoïdes contenant du Mn étaient également inhibés aux températures lorsque les dispersoïdes d'$Al_3(Sc,Zr)$ commençait à précipiter. L'effet combiné sur la résistance à la recristallisation a également été étudié sur les échantillons laminés à chaud après un traitement de préchauffage à 400 ℃ pendant 2 heures. Les résultats ont montré que la seule addition de Zr entraînait une aggravation de l'inhibition de la recristallisation, tandis que l'addition combinée de Zr et de Sc augmentait l'inhibition de la recristallisation par rapport à l'base de l'alliage Al-Mg-Si 6082.

ABSTRACT

To satisfy the increasing demand for aluminum alloys to be applied at high temperatures or transformed into desired shape without sacrificing the mechanical strength, the improvement of elevated-temperature properties and recrystallization resistance during hot deformation and annealing is very important. The present work was taken to achieve both goals by introducing dispersoids through addition of transition elements, such as Mn, Zr and Sc. Though extensive work has been done on this topic, there are still several aspects that need further clarification, namely the effects of the transition elements and their interaction as well as the heat treatments. Therefore, Mn, Zr and Sc were added into Al-Mg-Si 6082 alloys to perform the investigations.

As the first step, the precipitation behavior of Mn-containing dispersoids in Al-Mg-Si 6082 alloy with various Mn contents (up to 1 wt.%, all the composition is shown in wt.% unless indicated otherwise) during various heat treatment procedures (300-500 ℃) has been systematically studied. Meanwhile, the role of dispersoids on elevated-temperature strength and recrystallization resistance during hot-rolling and annealing has been dealt with. Results showed that, regardless of the Mn contents, the dispersoids began to precipitate at 350 ℃ and reached to the optimum condition after 2 hours at 400 ℃, leading to the highest microhardness at room temperature and yield strength at 300 ℃. However, they are gradually coarsening at temperatures above 450 ℃. The increase of Mn from 0.5% to 1.0% generally increases the number

density of dispersoids but the evolution of size is greatly related to the temperature. They are similar in the alloys with 0.5 and 1.0% Mn contents at lower temperature (<=400 ℃) while the coarsening rate of dispersoids in the alloy with 1.0% Mn is much higher at higher temperature (>450 ℃). During the annealing process after hot-rolling, the presence of Mn-containing dispersoids was found to significantly improve the recrystallization resistance though the recrystallization volume increases with annealing time in all experimental alloys. In addition, superior recrystallization resistance was obtained in the alloy containing 0.5% Mn (compared to the alloy with high Mn addition (1.0%), which was attributed to its slower coarsening rate of dispersoids during annealing and larger original grain size before rolling.

Based on the results obtained above, additional Zr and Sc elements were added into the alloy containing 1.0% Mn to study the effect of Zr and Sc addition on Mn-containing dispersoids under various heat treatment conditions and interactions between Al_3Zr, $Al_3(Sc,Zr)$ and Mn-containing dispersoids. It was found that the individual Zr addition and the combined Sc and Zr addition had different influences on Mn-containing dispersoids as a function of heat treatment temperature. At 350 ℃, the combined Zr and Sc addition significantly suppressed the precipitation of Mn-containing dispersoids while the effect of the individual Zr addition on Mn-containing dispersoids was much less prominent. At 400 ℃, the individual Zr addition inhibited the precipitation of Mn-containing dispersoids but negligible effect was observed with the combined Zr and Sc additions. At 450 ℃, however,

Mn-containing dispersoids was not suppressed any more in both cases. The mechanism leading to such phenomena was attributed to the preferential nucleation of Al_3Zr dispersoids on u-phase and simultaneous consumption of the latter, thus preventing the precipitation of Mn-containing dispersoids, which also preferred to nucleate on u-phase. Similar reason was expected to apply to Al_3(Sc,Zr) dispersoids, since Mn-containing dispersoids were also inhibited at temperatures when Al_3(Sc,Zr) started to precipitate. Their combined effect on the recrystallization resistance was also investigated on the hot-rolled samples after pre-heat treatment at 400 ℃ for 2 hours. The results showed that, the sole addition of Zr led to a worse recrystallization inhibition while the combined addition of Zr and Sc enhanced the recrystallization inhibition compared to the base Al-Mg-Si 6082 alloy.

TABLE OF CONTENTS

LIST OF FIGURES

LIST OF TABLES

Acknowledgements

Here I sincerely thank everyone who encouraged and supported me during my master study at University of Quebec at Chicoutimi (UQAC).

First of all, I would like to show my gratitude to Professor X. Grant Chen for offering me a chance to study in Canada. His passion to the research work and to the life deeply inspired me. Also, I would like to express my thanks to my co-supervisor Professor Kun Liu. He regarded me more like a co-worker than his student. We usually discussed on some scientific issues “intensively”, and by doing so he corrected many of my incorrect but stubborn opinions and encouraged me to promote new and more solid ideas. I also would like to thank Professor Zhan Zhang, for the training of SEM and TEM and also for the little chat each time I felt stressful. I am also very grateful to Professor Sarkar Dilip who gave me wonderful courses at my first two semesters and invited me several times for the delicious dinner.

Secondly, I would like to thank my friends and colleagues in CURAL, Sinan Chen, Mengyun Liu, Anil, Zhixing Chen, Xingli Chen, Dong Li, Shuai Wang, Dr. Zhen Li, Jian Qin and Lanfeng Jin, who offered me lots of help in both academic field and my life in Chicoutimi. Also I would like to thank our technicians for the support of our experiments in CURAL.

Finally, I would like to thank my girlfriend and future wife Wei Xu, for her everlasting support and companion.

CHAPTER 1

INTRODUCTION

1.1 Background

The Al-Si-Mg 6xxx aluminum alloys are one of the most widely used wrought alloys in the aerospace, automotive and construction industries due to their strength to weight ratio and high corrosion resistance. Recently, there are increasing demands for aluminum alloys to be applied at elevated temperatures (250-300 ℃) in the aerospace automobile industries. However, their mechanical properties deteriorates rapidly at elevated temperatures due to the coarsening of traditional hardening precipitates Mg_2Si at 250-300 ℃ [1]. On the other hand, these alloys are usually subjected to the thermal-mechanical deformation, such as rolling and extrusion, in order to achieve desirable shape. The occurrence of recrystallization during hot deformation inevitably weakens the mechanical strength of the final products. Therefore, studies concerning about enhancing elevated-temperature properties and recrystallization resistance of 6xxx alloys are of great importance.

Introducing the thermally stable dispersoids via the addition of transition elements, such as Mn, Zr and Sc after appropriate heat treatments, is reported to be one of the most efficient and applicable approaches to improve the elevated-temperature

properties. It is reported that the Yield Strength (YS) at 300 ℃ of Al-Mg-Mn 3004 alloys has been improved to 78 MPa compared to 55 MPa after homogenization and the mechanical properties were stable during the service time at 300 ℃ due to the formation of high volume of dispersoids with excellent thermal stabilities [2]. In addition, the dispersoids are also reported to inhibit the recrystallization occurred during hot deformation and subsequent annealing by exerting Zener-drag on the moving grain boundaries [3-8]. Vladivoj and Margarita [9] even achieved fully stagnated recrystallization during annealing for 8 hours at 520 ℃, with alloys containing 0.25% Sc and 0.08% Zr. Meanwhile, the efficiency of these dispersoids was found to be highly depended on their size and distributions [10, 11]. In general, dispersoids with finer size and denser distributions contribute to the superior strength at elevated temperatures and have a high inhibition effect on recrystallization. On the other hand, the distribution of dispersoids was strongly dependent on the heating rate during heat treatment. R. Hu *et al.* [4] found that a rapid heating rate produced needle-shaped heterogeneous dispersoids while a slow heating rate produced fine and evenly distributed dispersoids in the Al-Fe-Mn-Si alloy. Similar phenomena has also been observed in AA7010 alloys that Al_3Zr tended to form coarser dispersoids when a fast heating rate was applied [12].

However, few studies have been performed in 6xxx alloys on the influence of heat treatment on the formation and distribution of dispersoids. In addition, although a large body of works has addressed the effect of the secondary particles and

dispersoids on recrystallization during annealing with regard to the phenomena of Zener pinning [13-17], little work has been performed to consider the evolution of the influence of dispersoids on the recrystallization during hot deformation and annealing process. However, it is expected that the change on the characters of dispersoids and precipitates will definitely affect the Zener-drag force during the annealing process, especially at relatively high temperature annealing process [18]. Meanwhile, the introduction of dispersoids from different families has recently become a trend in order to further enhance the properties of the alloys but the results turned out to be controversial [19-21]. Therefore, the clarification of these issues mentioned above will be of great importance.

In the present study, the research focused on the effects of transition elements, such as Mn, Zr and Sc, as well as heat treatment parameters on the microstructure and mechanical properties of AA6082 alloys. The interactions between dispersoids induced by these elements and their combined effect were also studied.

1.2 Objectives

The general objective of this thesis was to develop 6xxx alloys with superior mechanical properties, especially high elevated-temperature strength and recrystallization resistance through the precipitation dispersoids induced by transition

elements. Therefore, Mn, Zr and Sc were added into AA6082 alloys to achieve the following objectives:

1. To systematically study the effect of heat treatment parameters on distribution of Mn-containing dispersoids.
2. To address the influence of various Mn contents on elevated-temperature properties and recrystallization resistance.
3. To clarify the individual addition of Zr and the combined Zr and Sc on the formation of dispersoids, microstructure and mechanical properties under different heat treatments.
4. To investigate the interactions occurred between different types of dispersoids.

REFFERENCES

[1] M. Usta, M. Glicksman, and R. Wright, “The effect of heat treatment on Mg_2Si coarsening in aluminum 6105 alloy,” *Metallurgical and Materials Transactions A*, vol. 35, pp. 435-438, 2004.

[2] K. Liu, and X.-G. Chen, “Development of Al–Mn–Mg 3004 alloy for applications at elevated temperature via dispersoid strengthening,” *Materials & Design*, vol. 84, pp. 340-350, 2015.

[3] F. Hichem, and G. Rebai, “Study of dispersoid particles in two Al–Mg–Si aluminium alloys and their effects on the recrystallization,” *Applied Physics A*, vol. 119, pp. 285-289, 2015.

[4] R. Hu, T. Ogura, H. Tezuka *et al.*, “Dispersoid formation and recrystallization behavior in an Al-Mg-Si-Mn alloy,” *Journal of Materials Science & Technology*, vol. 26, pp. 237-243, 2010.

[5] P. Mukhopadhyay, M. Loeck, and G. Gottstein, “A cellular operator model for the simulation of static recrystallization,” *Acta materialia*, vol. 55, pp. 551-564, 2007.

[6] M. A. Somers, M. Somerday, and J. F. Humphreys, "The effect of dispersoids on the recrystallization behavior of a high-purity Al-1.3Mn alloy," *Trans tech publ*, vol. 331, pp. 703-714, 2000.

[7] S. Tangen, K. Sjølstad, T. Furu *et al.*, “Effect of concurrent precipitation on recrystallization and evolution of the P-texture component in a commercial

Al-Mn alloy," *Metallurgical and Materials Transactions A,* vol. 41, pp. 2970-2983, 2010.

[8] D. Tsivoulas, and P. Prangnell, "The effect of Mn and Zr dispersoid-forming additions on recrystallization resistance in Al–Cu–Li AA2198 sheet," *Acta Materialia,* vol. 77, pp. 1-16, 2014.

[9] V. Ocenasek, and M. Slamova, "Resistance to recrystallization due to Sc and Zr addition to Al–Mg alloys," *Materials Characterization,* vol. 47, pp. 157-162, 2001.

[10] F. J. Humphreys, and M. Hatherly, *Recrystallization and related annealing phenomena*: Elsevier, 2012.

[11] E. Nes, N. Ryum, and O. Hunderi, "On the Zener drag," *Acta Metallurgica,* vol. 33, pp. 11-22, 1985.

[12] B. Morere, R. Shahani, C. Maurice *et al.*, "The influence of Al_3Zr dispersoids on the recrystallization of hot-deformed AA 7010 alloys," *Metallurgical and Materials Transactions A,* vol. 32, pp. 625-632, 2001.

[13] A. Eivani, H. Ahmed, J. Zhou *et al.*, "Correlation between electrical resistivity, particle dissolution, precipitation of dispersoids, and recrystallization behavior of AA7020 aluminum alloy," *Metallurgical and materials Transactions A,* vol. 40, pp. 2435-2446, 2009.

[14] B. Forbord, L. Auran, W. Lefebvre *et al.*, "Rapid precipitation of dispersoids during extrusion of an Al–0.91 wt.% Mn–0.13 wt.% Zr–0.17 wt.% Sc-alloy," *Materials Science and Engineering: A,* vol. 424, pp. 174-180, 2006.

[15] I. Nikulin, A. Kipelova, S. Malopheyev *et al.*, “Effect of second phase particles on grain refinement during equal-channel angular pressing of an Al–Mg–Mn alloy,” *Acta materialia,* vol. 60, pp. 487-497, 2012.

[16] M. Somerday, and F. Humphreys, “Recrystallisation behaviour of supersaturated Al–Mn alloys Part 1–Al–1.3 wt-% Mn,” *Materials science and technology,* vol. 19, pp. 20-29, 2003.

[17] S. Tangen, H. Bjerkaas, T. Furu *et al.*, "The Effects of Dispersoids on the Recrystallization Behavior in a Cold Rolled AA 3103-Aluminium Alloy," *Materials Forum,* vol. 28, pp. 1229-1234, 2004.

[18] K. Liu, and X.-G. Chen, “Influence of heat treatment and its sequence on elevated-temperature properties of Al-Mn-Mg 3004 alloy,” *Materials Science and Engineering: A,* vol. 697, pp. 141-148, 2017.

[19] M. Conserva, and M. Leoni, “Effect of thermal and thermo-mechanical processing on the properties of Al-Mg alloys,” *Metallurgical Transactions A,* vol. 6, pp. 189-195, 1975.

[20] S. W. Cheong, and H. Weiland, "Understanding a microstructure using GOS (grain orientation spread) and its application to recrystallization study of hot deformed Al-Cu-Mg alloys." *Trans tech publ,* vol. 558, pp. 153-158, 2007.

[21] M. J. Starink, N. Gao, N. Kamp *et al.*, “Relations between microstructure, precipitation, age-formability and damage tolerance of Al–Cu–Mg–Li (Mn, Zr, Sc) alloys for age forming,” *Materials Science and Engineering: A,* vol. 418, pp. 241-249, 2006.

CHAPTER 2

LITERATURE REVIEW

2.1 Development of Al-Mg-Si aluminum alloys

Al-Mg-Si alloys are an important group of alloys that are widely used in both cast and wrought forms [1]. Among them, AA6xxx series are one of the most commonly applied groups in structural components and industrial sections due to their high strength/weight ratio, good corrosion resistance and low cost [2, 3]. They are precipitation-hardening alloys and are generally undergoing T6 heat treatment to achieve adequate strength. Extensive research has been performed on the precipitation sequence in Al-Mg-Si alloys and it is generally acknowledged that the decomposition of Al-Mg-Si supersaturated solid solution (SSSS) is a five-stage process, [4-6], i.e.,

$$SSSS \rightarrow Mg/Si\ clusters \rightarrow GP\ zones \rightarrow \beta'' \rightarrow \beta' \rightarrow \beta - Mg_2Si$$

The early stage of aging leading to formation of Mg/Si clusters concerns a rather complex and controversial phenomenon [7-9]. Some researchers have suggested that clusters of Mg and Si form independently during the earliest stage of precipitation [10]

while the others have hypothesized that Si-rich clusters aggregate first followed by the coarsening and Mg-enrichment [2].

The earliest precipitates which produce a distinguishable contrast from transmission electron microscopy (TEM) characterization are GP zones [11]. These precipitates, having spherical shape and typical size of 1-3 nm, are more thermally stable than Mg/Si clusters and have been reported to transform to β'' phase in the later sequence [11-15].

The β'' precipitates, which mainly forms during medium stage of aging [16-19], has been the subject of much interest since they are associated with peak aged conditions and thus responsible for the highest strength. These precipitates, which have the base-centered monoclinic structure, are fine needle-like and aligned along $<001>_{Al}$, being fully coherent only along the needle axis. The chemical composition of the β'' phase has been proposed as Mg_5Si_6 [14, 20], however, it has been clarified in the past few years that the exact composition of β'' is highly dependent on the specific composition of each individual alloy [13, 21, 22].

β' precipitates form in over-aged condition after β'' precipitates in the aging sequence. They are rod shaped and still aligned along $<001>_{Al}$ [23-25]. The structure has been determined by Jacobs [25] to be hexagonal. Although the composition of this phase has also been analyzed, the results are not conclusive. Lynch *et al.et al.* [26]

obtained the Mg:Si atomic ration as low as 0.44 while Matsuda *et al.et al.* [27] determined the Mg:Si ratio to be 1.68 through an energy dispersive spectrometer (EDS). In addition, lath-shaped B' phase which possesses a crystal structure of orthorhombic or hexagonal is also reported to precipitate associated with β' phase along $<001>_{Al}$ [28].

Platelet equilibrium β phase is the last one formed in the aging sequence. It has been established to be of the fluorite structure with a Mg/Si ratio of 2:1, which has negligible hardening contribution [1].

Relatively few reports have documented the precipitation kinetics of Mg_2Si during and/or after deformation [29-32]. It has been reported that the implement of deformation as part of the heat treatment process can significantly affect the age hardening of AA6xxx alloys [29, 30]. Though highly depending on the extent of deformation, some results suggest that dislocations induced by deformation have a significant influence on the formation of GP zones and the nucleation/growth of the intermediate phase [29-32].

2.2 Introduction of dispersoids via transition elements

2.2.1 Mn-induced dispersoids

Recently, there are increasing demands for Al-Mg-Si 6xxx alloys to be applied at elevated temperatures (250-300 ℃) in automobile industries. However, their mechanical properties deteriorates rapidly at elevated temperatures due to the coarsening of traditional precipitates β'' at 250-300 ℃. Meanwhile, these alloys are usually applied in wrought forms, such as rolling and extrusion products, in order to fulfil multiple functions. Therefore, studies concerning about enhancing elevated-temperature properties of 6xxx alloys and recrystallization resistance during hot deformation are of great importance.

Introducing the thermal stable Mn-containing dispersoids via Mn addition and appropriate heat treatments is reported to be one of the most efficient and applicable approaches to enhance the elevated-temperature properties, especially in AA3xxx alloys. By inducing Mn dispersoids, the Yield Strength (YS) at 300 ℃ of 3004 alloys has been significantly improved compared to the alloy after homogenization and the mechanical properties were stable during the service time at 300 ℃ [33]. After optimizing contents of Si and Mg, Zhen Li *et al.* [34] achieved even superior improvement in elevated-temperature yield strength and creep resistance over alloys

free of Mg and Si in 3xxx alloys through Mn-containing dispersoids since a larger volume fraction of dispersoids have been obtained. Since studies concerning about improving elevated-temperature strength in AA6xxx alloys through introduction of Mn-containing dispersoids have been scarce, application of Mn additions in AA6xxx alloys in order to improve elevated-temperature properties is expected to be more promising since AA6xxx alloys are more readily applied in aerospace and automotive industries.

On the other hand, the Mn-containing dispersoids are also reported to have a controversial influence on the recrystallization behaviors occurred during deformation and subsequent annealing. Relatively large needle shaped Mn-containing dispersoids formed by rapid pre-heating to 530 ℃ are reported to significantly accelerate the recrystallization process by Rong *et al.* [35]. While Richard *et al.* [36] claim that the Mn-containing dispersoids formed during the pre-heating to 560 ℃ with a slow heating rate of 50 ℃/h severely resist the recrystallization process occurred during hot-rolling at 440 ℃ and the following annealing at 560 ℃ in AA6013 alloys. They also proposed that the higher the Mn content is, the more effective the resistance to recrystallization will be. The complicated influence on the overall recrystallization characteristics of deformed alloy is attributed to the inter-particle spacing and particle size of Mn-containing dispersoids [37, 38]. Small dispersoids give rise to a more homogenous distribution of dislocations thus decreasing the preferential nucleation sites for recrystallization and a short inter-particle spacing induce a large Zenner drag

on the re-arrangement of the subgrains, therefore retarding both the nucleation and growth of the recrystallized grains. While large needle shaped dispersoids tend to act as preferential nucleation sites for recrystallized grains since regions with high dislocation density was introduced at particle-matrix interfaces [39]. In addition, the pinning force induced by coarse and sparse dispersoids is rather small, thus accelerating the overall recrystallization. Though the recrystallization behavior has been exhaustively discussed, systematic study on the recrystallization resistance effect of Mn-containing dispersoids is still far from systematic, especially in AA6xxx alloys. For instance, the pre-heat treatment temperatures employed in the literature [3,4,7] are all above 530 ℃, during which the dispersoids were expected to coarsen quickly, thus will significantly decrease the Zener-pinning effect compared with the optimum distribution. Besides that, the evolution of dispersoids during post-deformation annealing is not considered, which would also affect the Zenner-drag force. K. Huang *et al.* [40] took the concurrent precipitation of dispersoids during recrystallization into consideration and concluded that, the concurrent precipitated dispersoids contribute to the resistance of recrystallization while the pre-existing dispersoids coarsen and give rise to the particle stimulated nucleations (PSN). However, the pre-existing and concurrent precipitated dispersoids cannot be affectively distinguished since the annealing temperature is as low as 350 ℃ and with a rather slow heating rate (50 ℃ /h).

The as-cast microstructure of AA6082 alloys is clearly demonstrated in Fig. 2.1a. It can be seen that there are generally two kinds of phases observed, namely primary Mg_2Si phases (indicated by arrow A) and Mn-Fe containing phases (indicated by Arrow B). While after proper heat treatment and chemical etching, zones of Mn-containing dispersoids and precipitation free zones (PFZ) can be revealed. As indicated in Figs. 2.1b and c, PFZ turns to distribute on dendrite cores and boundaries, which is resulted from the segregation of Mn solutes during solidification and strong Mn depletion around Mn-Fe containing phases [41]. The crystallographic nature of Mn-containing dispersoids in Al-Mg-Si alloys have also been investigated and referred to be α-Al(FeMn)Si dispersoids [42-49]. However, there is still on-going discussion whether the structure is simple cubic (SC) or body center cubic (BCC). Several researches indicate that the unit cell is SC when the Fe/Mn ratio is low and becomes BCC when Fe/Mn ratio becomes higher [45, 46].

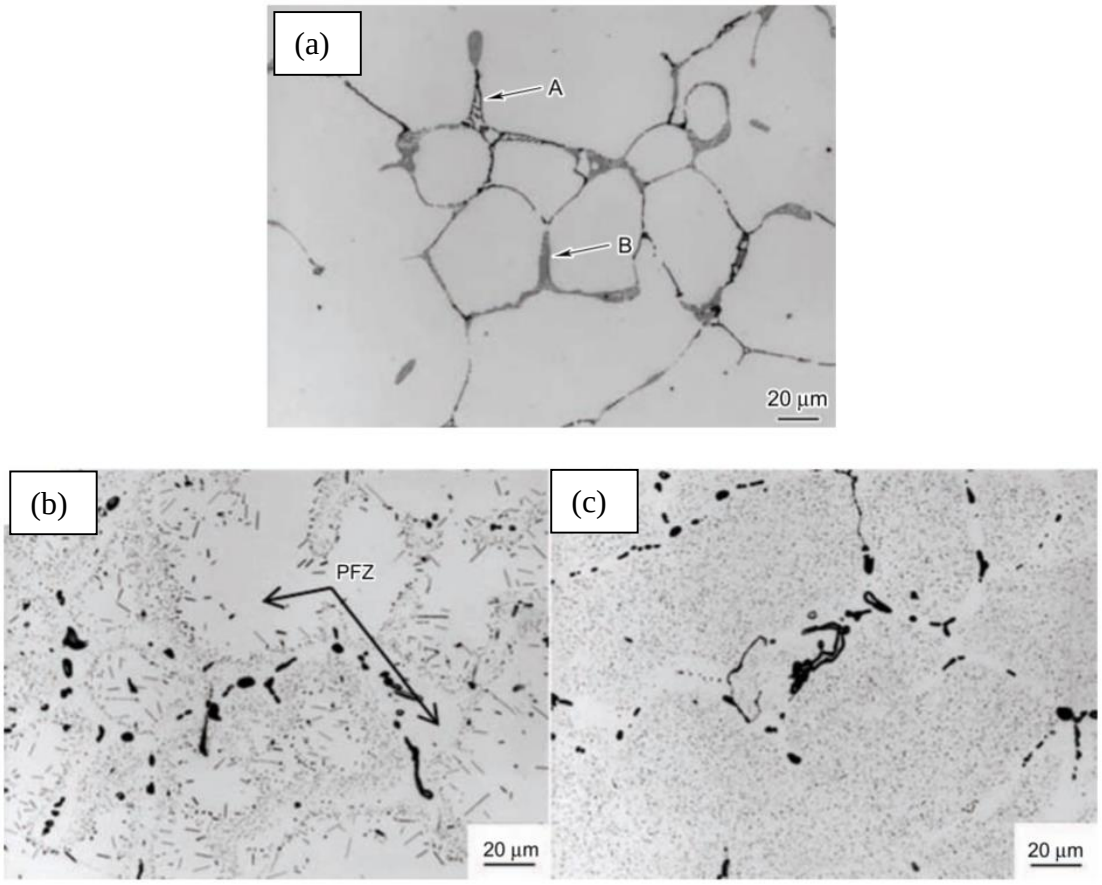

Fig. 2.1 Optical micrograph for (a) the as-cast 6082 alloy showing crystallized intermetallic compounds and after homogenization at 530 ℃ with (b) rapid heating and (c) slow heating [35].

Extensive works have been applied to investigate the formation of Mn-containing dispersoids in Al-Mg-Si alloys [17-19].

The distribution of Mn-containing dispersoids is reported to be highly dependent on the heating rate [3, 16]. For instance, after heating two identical 6082 alloys to 530 ℃ with two different heating rates, Rong. H *et al.* [35] found that a rapid heating rate produces large needle shaped heterogeneously distributed dispersoids (Fig. 2.1b),

while a slower heating rate produces fine spherical shape dispersoids with a more homogeneous distribution (Fig. 2.1c). Nevertheless, PFZ can hardly be completely eliminated.

Hirasawa [50] provided some evidence that β'' and β' phase formed during the heating process can act as nucleation sites for the Mn-containing dispersoids during high temperature annealing by pointing out that Mn-containing dispersoids have the same crystal habit plane as Mg_2Si. Even β-Mg_2Si platelets have been suggested as nucleation sites. Lodgaard and Ryum [51] have found an intermediate phase with respect to Mn-containing dispersoids, referred to as 'u-phase', nucleates on the β'-Mg_2Si needles during the heating to 580 ℃, suggesting that only the 'u-phase' precipitates act as nucleation sites for the dispersoids. This 'u-phase' was semi-coherent with the Al lattice on [100] Al direction and has also been found by Reiso *et al.* [19] with equiaxed shape, the diffraction pattern of which was shown in Fig. 2.2. The diffraction pattern of $<001>_{u\text{-}phase}$ can be clearly seen.

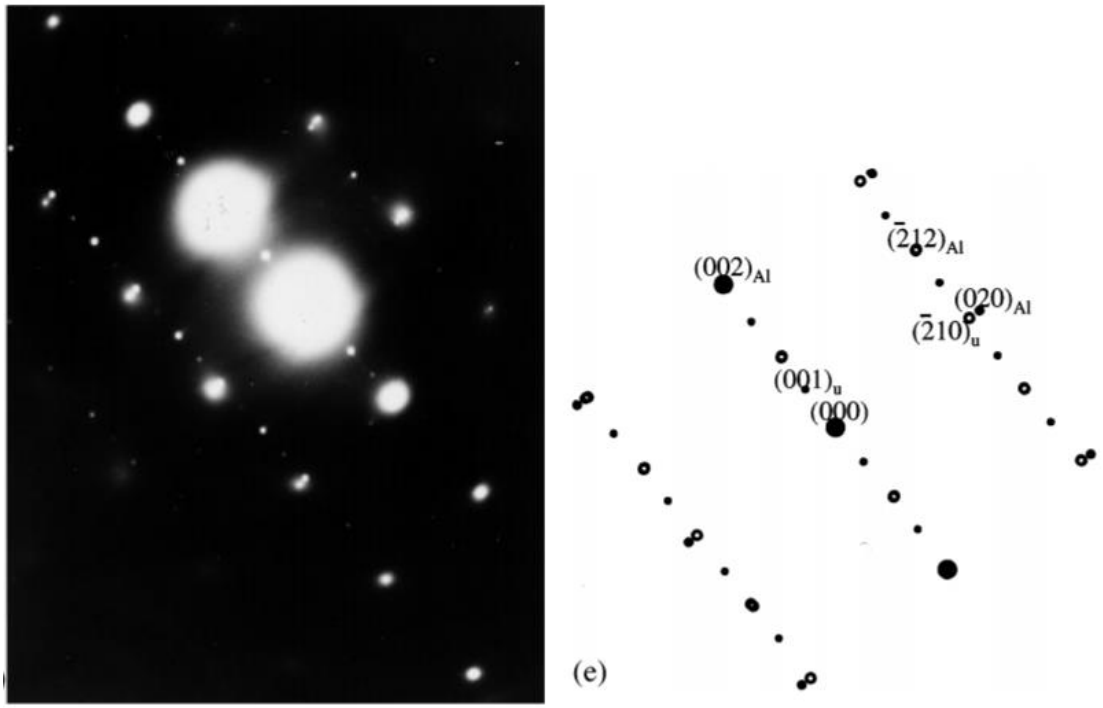

Fig. 2.2 (a) Electron diffraction pattern from the 'u-phase' precipitate taken along the [120]'u-phase' direction and (b) Indexing of the diffraction pattern shown in (a) [51].

2.2.2 Zr (and Sc)-containing dispersoids

Small quantities of Zr or combined Zr and Sc additions are also commonly added into a wide range of aluminum alloys to achieve better recrystallization resistance and mechanical properties. It has been widely reported that, Al alloys with Zr additions can retain their deformed structure and prevent recrystallization, as well as enhance mechanical properties through a proper precipitation heat treatment [52-54]. To further improve the effect of resistance to recrystallizations, some approaches to

stepwise homogenization were explored in the literature [55-57]. For instance, Zhanying *et al.* [57] have achieved a remarkable reduction of recrystallization volume fraction through a two-step heat treatments with the first step in the temperature range of 300-400 ℃ followed by the second step at 470 ℃. Combined addition of Sc with Zr has been reported to be another viable approach to improve the inhibition to recrystallization [58-61]. Jia *et al.* [60] have designed a set of Al-Zr-Sc alloys with various Sc contents ranging from 0 to 0.15% and observed the recrystallization inhibition effects to be proportional to the additional Sc after pre-heat treatment at 475 ℃ for 12 hours. Vladivoj and Margarita [58] even achieved fully stagnated recrystallization when annealed for 8 hours at 520 ℃, with alloys containing 0.25% Sc and 0.08% Zr.

A large body of works has addressed the precipitation behaviors of Al_3Zr and $Al_3(Sc,Zr)$ dispersoids due to the addition of Zr and/or Sc. During post-solidification aging, decomposition of supersaturated Al-Zr solid solutions occurs initially by the formation of nanometer-scale Al_3Zr dispersoids with a metastable cubic $L1_2$ structure, which transform to the equilibrium $D0_{23}$ phase after prolonged aging at temperatures above 450 ℃ [62-65]. In addition, nano-scaled Al_3Zr ($L1_2$) dispersoids have been found to have a remarkable hardening response at temperatures from 375 to 425 ℃ and there is no appreciable overaging effect despite extended the aging times at 425 ℃ until the temperatures go above 450 ℃ [66], when the meta-stable $L1_2$ Al_3Zr dispersoids transform to their equilibrium $D0_{23}$ structures [67]. However, the

application of Al_3Zr dispersoids as inhibitors for recrystallization was still limited due to their severely heterogeneously distribution, since the ineligible dispersoids free regions are rendered more prone to recrystallization due to the localized reduction in Zenner pinning. There are several reasons reported for the heterogeneity of Al_3Zr dispersoids. The first and primary reason is the severe microsegregation of Zr solute atoms during solidification [68]. Since Zr forms a terminal peritectic with Al and the equilibrium partition coefficient for solidification, k_0, is greater than unity, the first solid to form during solidification is therefore richer in Zr compared to the bulk alloy composition, resulting in solute-rich dendritic cores surrounded by solute-depleted interdendritic channels. Thus, large quantities of Al_3Zr dispersoids precipitate inside dendrite cores while the dendrite boundaries remained free during precipitation annealing, as shown in Fig. 2.3. However, the microsegregation of Zr can hardly be eliminated by the homogenization due to the low diffusion rate of Zr solute atoms [69].

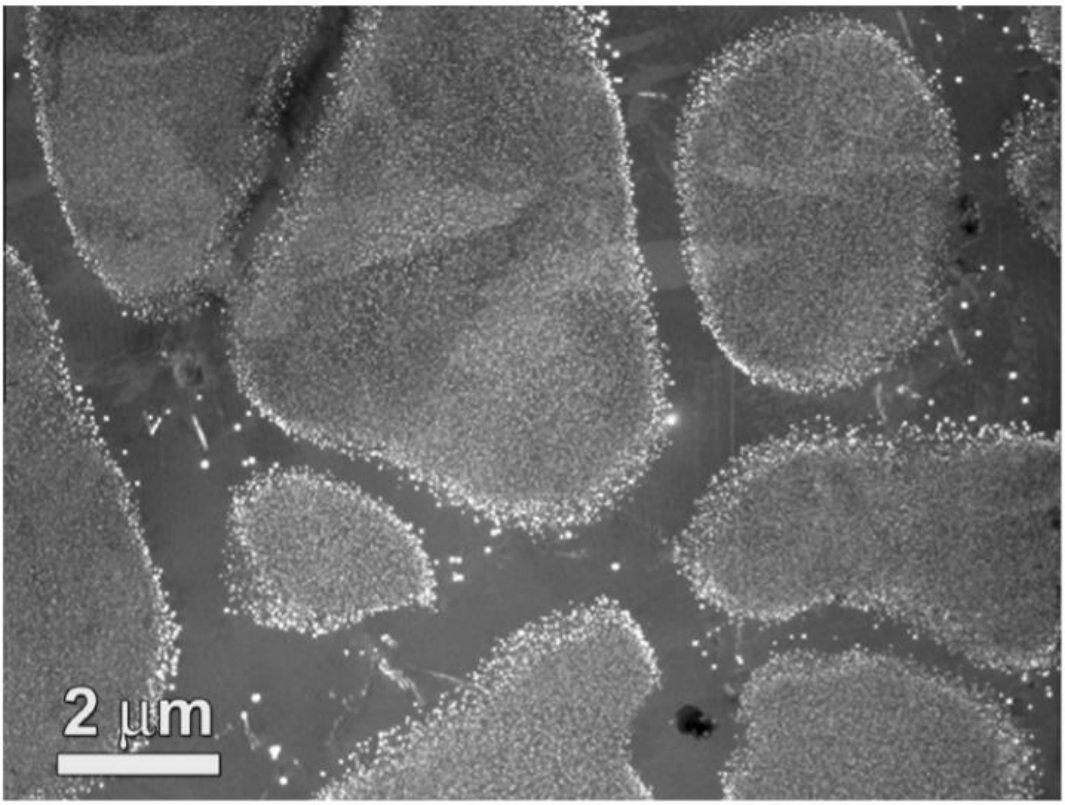

Fig. 2.3 Centered dark-field transmission electron micrograph of an Al– 0.1Zr–0.1Ti (at.%) alloy aged at 375 ℃ for 1600 h, exhibiting an inhomogeneous dendritic distribution of Al_3Zr precipitates [66].

Another reason responsible for the heterogeneous distribution of Al_3Zr dispersoids is their nucleation preferential sites. Robson and Prangnell [70] have proposed that Al_3Zr dispersoids prefer to nucleate on the η' phase in the dendrite regions of an AA7050 alloy. On the other hand, Jia *et al.* [71] reported the presence of helical and lath clusters of Al_3Zr dispersoids oriented along $<001>_{Al}$ and attributed them to the preferential nucleation on dislocations and other strengthening phase respectively. The final but not the last reason is their inclusion in various types of particles, for

instance $Al_{20}Cu_2Mn_3$, Al_3Cr, Al_6Mn and $Al_7Cu_3Zr_2$ in different alloys [72-74], which can also have a detrimental effect to the final distribution.

Combined addition of Sc with Zr has drawn much attention since it transformed the former heterogeneous distribution of Al_3Zr dispersoids into rather homogenous $Al_3(Sc,Zr)$ [75-77]. One significant reason is that Sc solute forms a terminal eutectic with Al and has a partition coefficient, k_0, close to unity, which compensate very well with Zr. Moreover, due to the similar physical and chemical properties of Zr and Sc, the combined addition of Zr and Sc can lead to the formation of self-complementary Al_3Sc ($L1_2$), Al_3Zr ($L1_2$) and $Al_3(Sc,Zr)$ ($L1_2$) dispersoids [78, 79], as shown in Fig. 2.4.

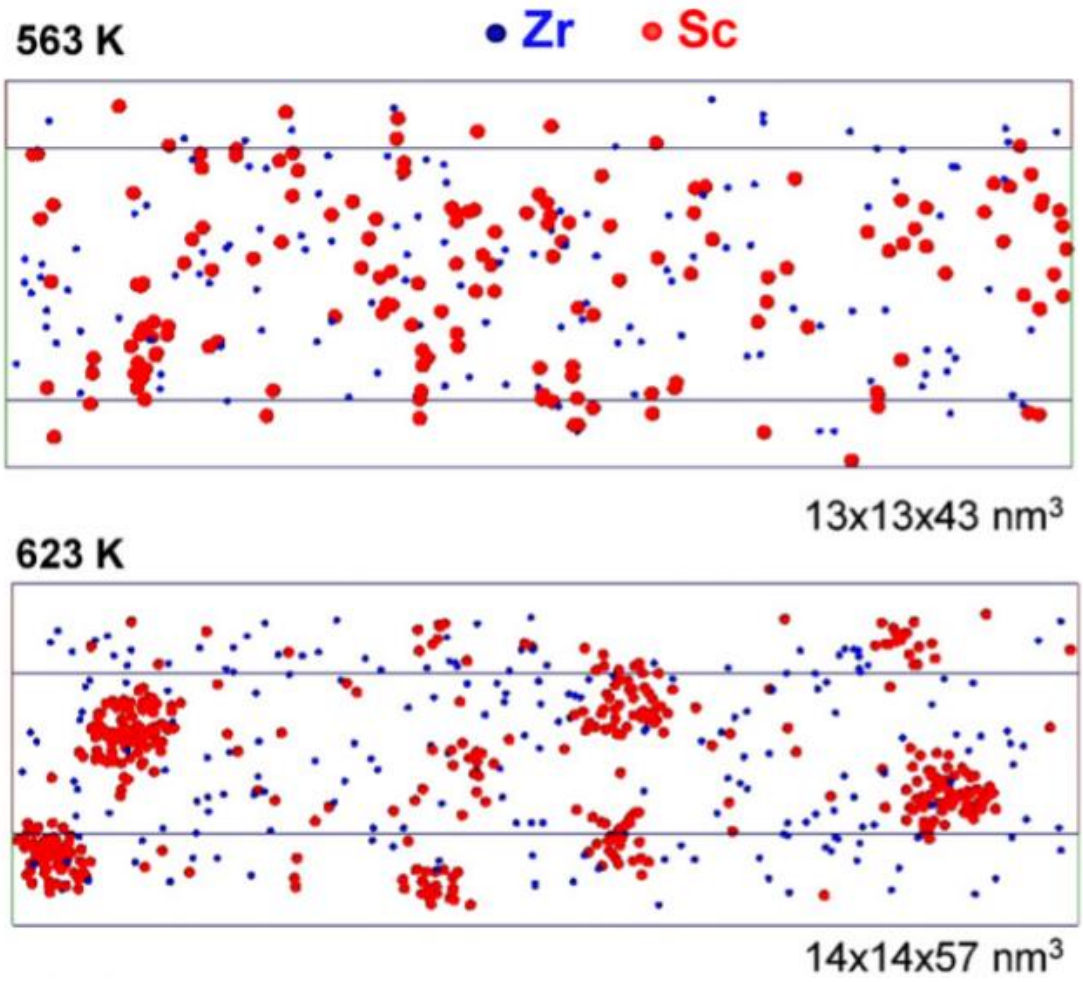

Fig. 2.4 3D reconstructions of specimen as analyzed by APT. The distribution of Sc and Zr atoms is displayed for the two investigated temperatures at which the heating ramp was stopped and immediately followed by a water quench [80].

The generally accepted precipitation kinetics of $Al_3(Sc,Zr)$ dispersoids during the heat treatment can be summarized as follows [80]:

$$\text{Sc} - \text{rich clusters} \rightarrow \text{Al}_3\text{Sc particles} \rightarrow \text{Al}_3\text{Sc enriched in Zr at the interface}$$

$$\rightarrow \text{Al}_3\text{Sc core} + \text{Al}_3(\text{Sc}_x\text{Zr}_{1-x})\ \textit{shell}$$

Where a homogenous Al_3Sc distribution forms first due to the relative fast diffusion rate of Sc, followed by the segregation of Zr on the interface of Al_3Sc cores and the final $Al_3Sc/Al_3(Sc,Zr)$ core/shell structure [81, 82]. Due to the existence of Zr shell, $Al_3(Sc,Zr)$ dispersoids also possess superior thermal stability [83-85]. Another advantage of combined Sc and Zr additions is that Sc could stabilize the $L1_2$ structure of Al_3Zr and delay their transformation to the equilibrium $D0_{23}$ structures [86].

2.3 Interactions between addition of transition elements

As mentioned in the section 2.1 and 2.2, PFZ of Mn-containing dispersoids tends to form on dendrite boundaries and cores, while Zr solutes, due to the high k value and large misfits with Al matrix, tended to segregate on dendrite cores and boundaries, thus decomposed in the form of Al_3Zr dispersoids on these preferential sites. Further addition of both Zr and Sc can lead to homogeneous distribution of Al_3(Sc,Zr) dispersoids which are also promising to complement with Mn-containing dispersoids. Therefore, combined addition of Mn and Zr, (Sc) can be theoretically beneficial.

However, the actual effects of combined Mn and Zr, (Sc) additions were controversial due to the complicated interactions between dispersoids from different families , such as Mn-containing dispersoid, Al_3Zr and Al_3(Sc,Zr) [87-89]. Conserva et Leoni [87] have found that, combined additions of Mn and Zr into Al-Mg-Si-Fe aluminum alloys result in a higher yield strength after performing pre-heat treatment at 440 ℃ for 24 hours before hot-rolling. Cheong et Weiland [88] also achieved superior resistance to recrystallization with combined Mn and Zr additions into Al-Cu-Mg alloys after hot deformation and annealing. Starink *et al.* [89], however, claim that, alloys with combined Zr and Mn additions are detrimental compared with solo Mn addition on terms of yield strength after hot-rolling at the conventional homogenization temperature in Al-Cu-Mg-Li alloys after pre-heat treating. Nevertheless, limited discussion has been made in literatures on this disagreement. In order to overview the

combined effect of Mn and Zr additons on mechanical properties and recrystallization resistance, Tsivoulas *et al.* [72] have made a chart characterizing their claimed influence taken from his own work and the literatures, as shown in Fig. 2.5, revealing an interdependence between the Zr and Mn content. Indication has also been made that more Mn additions are required than Zr to achieve beneficial effects. Several other important factors, such as pre-deformation heat treatment parameters, annealing temperatures, etc. affecting the combined effect of Mn and Zr, (Sc) additions, however, are rarely discussed. The most critical factor among them is the pre-heat treatment parameters applied, since they have a direct influence on the formation of all types of dispersoids.

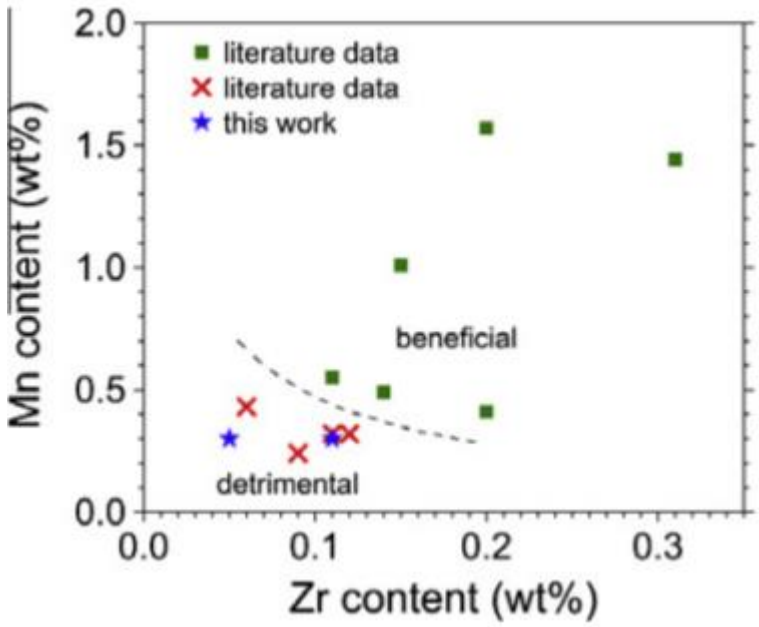

Fig. 2.5 Overview of the effect of combined Zr and Mn additions in various Al alloys taken from the literature, characterizing their claimed influence on recrystallization resistance [72].

Several works have addressed potential interactions between Mn and Zr, (Sc) additions [69, 90-92]. For instance, it has been reported that the presence of Zr resulted in fewer and coarser Mn-containing dispersoids in binary Al-Mn alloys [69, 90]. On the other hand, Mn additions have been observed to lead to the increase of volume fraction of Al_3Zr and $Al_3(Sc,Zr)$ dispersoids [69, 91, 92]. However, proposition has also been made that there is a negligible effect of joint additions of Mn, Zr and Sc, since neither dispersoid families were observed to show any difference when both elements were present [93].

Inclusion of element in the respective other precipitation phases, especially inclusion of Zr in various types of particles, has been reported to be one of the main reasons resulting in their interactions [70, 72, 74]. Kaibyshev *et al.* [74] has addressed enrichment of Zr in Al_6Mn and Al_3Cr dispersoids in the AA5083 alloys after homogenization at 520 ℃ for 10 hours. Some Zr was also observed to be included in $Al_{20}Cu_2Mn_3$ dispersoids and θ'- Al_2Cu in an AA2198 sheet after heat treated at 505 ℃ for 12 hours [72]. Zr inclusion has also been found in η phase in the as-cast state in AA7xxx alloys [70]. More interestingly, after proper precipitation heat treatment for Al_3Zr dispersoids, some of their clusters have been observed to exhibit in the shape of θ'-Al_2Cu and η phase in AA2xxx and AA7xxx respectively, as shown in Fig. 2.6, which further confirmed that due to the Zr inclusion in other particles, Al_3Zr dispersoid prefers to nucleate on these particles at its precipitation temperature and meanwhile consumes the latter, which is one of the significant mechanism how they interact with other particles.

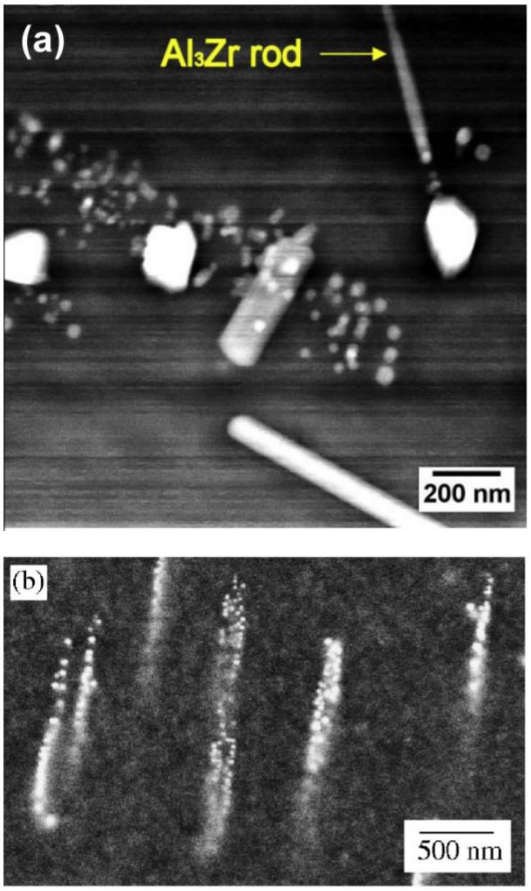

Fig. 2.6 Similarity in the shape of some Al_3Zr clusters with that of (a) θ'-Al_2Cu particles in AA2xxx alloys [94] and (b) η phase in AA7xxx alloys [70] after proper heat treatment.

Indeed, several works have been done to investigate interactions between Mn-containing dispersoids and Zr, (Sc)-induced dispersoids. However, researches concerning such interactions in AA6xxx alloys have been scarce. Meanwhile, very limited literatures have systematically addressed the effect of heat treatment temperatures on this interaction.

2.4 Recrystallization behaviors in aluminum alloys

There are several factors reported to have strong influence on the recrystallization behaviors of aluminum alloys, namely second phase particles, the original grain size and solutes [37]. Among those, the second phase particles, especially dispersoids, have the greatest inhibition effect of recrystallization in aluminum alloys by exerting the pinning effect (Zener drag) on boundaries. In 3xxx series aluminum alloys, Mn-containing dispersoids formed during homogenization are indicated to play an important role in controlling the recrystallization behavior [95]. In the case of 7xxx aluminum alloys, the formation of Sc- and Zr-containing dispersoids also has been a subject of interest for many years [96]. It was concluded that, by using the optimum heat treatment before deformation, a smaller fraction of recrystallization could be achieved.

In the literatures, the ratio of local volume fraction (F_v) and equivalent diameter (d) of the dispersoids is the most critical term, which determines the inhibition of both nucleation and growth of the recrystallizing grains. The limitation on the nucleation is given as the following equations [38],

$$\frac{F_v}{d} > \frac{2\alpha\Omega}{3\theta_m} \tag{2.1}$$

Where α is a constant, Ω is determined by local heterogeneities and θ_m is the angle to separate the high angle boundaries. The orientation gradient will tend to increase with a lager strain, therefore the critical value of F_v/d to suppress the nucleation will also increase with the increase of strain. Growth of the grains in such case is acted on by two composing pressures as shown in the following equation,

$$P = P_D - P_Z = \frac{3\gamma_s}{D} - \frac{3F_V\gamma_s}{d} \tag{2.2}$$

Where P_D is the driving force, P_Z is the pinning force, γ_s is the specific grain boundary energy, D is the diameter of the recrystallized grain [97]. Fv and d are the volume fraction and equivalent diameter of particles, respectively. Recrystallizing grains can only grow when P is positive, thus the stagnation of grain growth can be expected when F_v/d is larger than a critical value and vice versa.

REFERENCES

[1] G. Edwards, K. Stiller, G. Dunlop *et al.*, "The precipitation sequence in Al–Mg–Si alloys," *Acta materialia,* vol. 46, pp. 3893-3904, 1998.

[2] V. Fallah, B. Langelier, N. Ofori-Opoku *et al.*, "Cluster evolution mechanisms during aging in Al–Mg–Si alloys," *Acta Materialia,* vol. 103, pp. 290-300, 2016.

[3] F.-l. Zeng, Z.-l. Wei, J.-f. Li *et al.*, "Corrosion mechanism associated with Mg_2Si and Si particles in Al–Mg–Si alloys," *Transactions of Nonferrous Metals Society of China,* vol. 21, pp. 2559-2567, 2011.

[4] I. Dutta, and S. Allen, "A calorimetric study of precipitation in commercial aluminium alloy 6061," *Journal of Materials Science Letters,* vol. 10, pp. 323-326, 1991.

[5] M. Murayama, and K. Hono, "Pre-precipitate clusters and precipitation processes in Al–Mg–Si alloys," *Acta Materialia,* vol. 47, pp. 1537-1548, 1999.

[6] G. A. Edwards, K. Stiller, G. L. Dunlop *et al.*, "The precipitation sequence in Al–Mg–Si alloys," *Acta Materialia,* vol. 46, pp. 3893-3904, 1998.

[7] S. Pogatscher, H. Antrekowitsch, H. Leitner *et al.*, "Influence of interrupted quenching on artificial aging of Al-Mg-Si alloys," *Acta Materialia,* vol. 60, pp. 4496-4505, 2012.

[8] V. Fallah, A. Korinek, B. Raeisinia *et al.*, "Early-stage precipitation phenomena and composition-dependent hardening in Al-Mg-Si-(Cu) alloys," *Materials Science Forum*, pp. 933-938, 2014.

[9] V. Fallah, A. Korinek, N. Ofori-Opoku *et al.*, "Atomic-scale pathway of early-stage precipitation in Al-Mg-Si alloys," *Acta Materialia,* vol. 82, pp. 457-467, 2015.

[10] F. A. Martinsen, F. J. H. Ehlers, M. Torsæter *et al.*, "Reversal of the negative natural aging effect in Al-Mg-Si alloys," *Acta Materialia,* vol. 60, pp. 6091-6101, 2012.

[11] J. Buha, R. N. Lumley, A. G. Crosky *et al.*, "Secondary precipitation in an Al-Mg-Si-Cu alloy," *Acta Materialia,* vol. 55, pp. 3015-3024, 2007.

[12] M. Murayama, and K. Hono, "Pre-precipitate clusters and precipitation processes in Al-Mg-Si alloys," *Acta Materialia,* vol. 47, pp. 1537-1548, 1999.

[13] J. Buha, R. N. Lumley, and A. G. Crosky, "Precipitation and solute distribution in an interrupted-aged Al-Mg-Si-Cu alloy," *Philosophical Magazine*, vol. 88, pp. 373-390, 2008.

[14] S. J. Anderson, H. W. Zandbergen, J. Jansen *et al.*, "Aluminium alloys: their physical and mechanical properties," *Acta Mater,* vol. 46, pp. 3283, 1998.

[15] C. D. Marioara, S. J. Andersen, J. Jansen *et al.*, "The influence of temperature and storage time at RT on nucleation of the β″ phase in a 6082 Al-Mg-Si alloy," *Acta Materialia,* vol. 51, pp. 789-796, 2003.

[16] J. Buha, R. N. Lumley, and A. G. Crosky, "Precipitation and solute distribution in an interrupted-aged Al–Mg–Si–Cu alloy," *Philosophical Magazine,* vol. 88, pp. 373-390, 2008.

[17] J. Buha, R. N. Lumley, A. G. Crosky *et al.*, "Secondary precipitation in an Al–Mg–Si–Cu alloy," *Acta Materialia,* vol. 55, pp. 3015-3024, 2007.

[18] S. Pogatscher, H. Antrekowitsch, H. Leitner *et al.*, "Influence of interrupted quenching on artificial aging of Al–Mg–Si alloys," *Acta Materialia,* vol. 60, pp. 4496-4505, 2012.

[19] S. Pogatscher, H. Antrekowitsch, H. Leitner *et al.*, "Influence of the thermal route on the peak-aged microstructures in an Al–Mg–Si aluminum alloy," *Scripta Materialia,* vol. 68, pp. 158-161, 2013.

[20] H. W. Zandbergen, S. J. Andersen, and J. Jansen, "Structure determination of Mg5Si6:particles in Al by dynamic electron diffraction studies," *Science,* vol. 277, pp. 1221-1225, 1997.

[21] H. K. Hasting, W. Lefebvre, C. Marioara *et al.*, "Comparative study of the β″-phase in a 6xxx Al alloy by 3DAP and HRTEM," *Surface and Interface Analysis,* vol. 39, pp. 189-194, 2007.

[22] H. S. Hasting, A. G. Frøseth, S. J. Andersen *et al.*, "Composition of β″ precipitates in Al–Mg–Si alloys by atom probe tomography and first principles calculations," *Journal of Applied Physics,* vol. 106, pp. 123527, 2009.

[23] W. Smith, “The effect of reversion treatments on precipitation mechanisms in an Al-1.35 at. pct Mg_2Si alloy,” *Metallurgical Transactions,* vol. 4, pp. 2435-2440, 1973.

[24] G. Thomas, “THE AGING CHARACTERISTICS OF ALUMINUM ALLOYS ELECTRON TRANSMISSION STUDIES OF Al-Mg-Si ALLOYS,” *Inst. of Metals,* 1961.

[25] M. Jacobs, “The structure of the metastable precipitates formed during ageing of an Al-Mg-Si alloy,” *Philosophical Magazine,* vol. 26, pp. 1-13, 1972.

[26] J. Lynch, L. Brown, and M. Jacobs, “Microanalysis of age-hardening precipitates in aluminium alloys,” *Acta Metallurgica,* vol. 30, pp. 1389-1395, 1982.

[27] K. Matsuda, S. Tada, S. Ikeno *et al.*, “Crystal system of rod-shaped precipitates in an Al-1.0 mass% Mg_2Si-0.4 mass% Si alloy,” *Scripta metallurgica et materialia,* vol. 32, 1995.

[28] S. D. Dumolt, D. E. Laughlin, and J. C. Williams, “Formation of a modified β' phase in aluminum alloy 6061,” *Scripta Metallurgica,* vol. 18, pp. 1347-1350, 1984.

[29] D. C. Long, Y. Ohmori, and K. Nakai, “Effects of Cold Rolling on the Aging Kinetics in an Al–Mg–Si Based Commercial Alloy,” *Materials Transactions, JIM,* vol. 41, pp. 690-695, 2000.

[30] K. Matsuda, M. Terasaki, S. Tada *et al.*, "Effect of excess Si on age-hardening in deformed Al-Mg_2Si alloys," *Japan Institute of Light Metals, Journal,* vol. 45, pp. 95-100, 1995.

[31] J. Y. Yao, D. A. Graham, B. Rinderer *et al.*, "A TEM study of precipitation in Al–Mg–Si alloys," *Micron,* vol. 32, pp. 865-870, 2001.

[32] J. Dutkiewicz, and L. Litynska, "The effect of plastic deformation on structure and properties of chosen 6000 series aluminium alloys," *Materials Science and Engineering: A,* vol. 324, pp. 239-243, 2002.

[33] K. Liu, and X. G. Chen, "Development of Al–Mn–Mg 3004 alloy for applications at elevated temperature via dispersoid strengthening," *Materials & Design,* vol. 84, pp. 340-350, 2015.

[34] Z. Li, Z. Zhang, and X. G. Chen, "Microstructure, elevated-temperature mechanical properties and creep resistance of dispersoid-strengthened Al-Mn-Mg 3xxx alloys with varying Mg and Si contents," *Materials Science and Engineering: A,* vol. 708, pp. 383-394, 2017.

[35] R. Hu, T. Ogura, H. Tezuka *et al.*, "Dispersoid Formation and Recrystallization Behavior in an Al-Mg-Si-Mn Alloy," *Journal of Materials Science & Technology,* vol. 26, pp. 237-243, 2010.

[36] R. A. Jeniski, B. Thanaboonsombut, and T. H. Sanders, "The effect of iron and manganese on the recrystallization behavior of hotrolled and solution-heat-treated aluminum alloy 6013," *Metallurgical and Materials Transactions A,* vol. 27, pp. 19-27, 1996.

[37] E. Nes, N. Ryum, and O. Hunderi, "On the Zener drag," *Acta Metallurgica,* vol. 33, pp. 11-22, 1985.

[38] F. J. Humphreys, and M. Hatherly, *Recrystallization and related annealing phenomena*: Elsevier, 2012.

[39] E. Nes, "The effect of a fine particle dispersion on heterogeneous recrystallization," *Acta Metallurgica,* vol. 24, pp. 391-398, 1976.

[40] K. Huang, Y. Li, and K. Marthinsen, "Effect of heterogeneously distributed pre-existing dispersoids on the recrystallization behavior of a cold-rolled Al–Mn–Fe–Si alloy," *Materials Characterization,* vol. 102, pp. 92-97, 2015.

[41] Y. J. Li, and L. Arnberg, "Quantitative study on the precipitation behavior of dispersoids in DC-cast AA3003 alloy during heating and homogenization," *Acta Materialia,* vol. 51, pp. 3415-3428, 2003.

[42] D. Munson, "A clarification of the phases occurring in aluminium-rich aluminium-iron-silicon alloys, with particular reference to the ternary phase alpha-AlFeSi," *INST METALS J,* vol. 95, pp. 217-219, 1967.

[43] G. Phragmén, "On the phases occurring in alloys of aluminium with copper, magnesium, manganese, iron, and silicon," *Journal of the Institute of Metals,* vol. 77, pp. 489-551, 1950.

[44] A. Dons, "AlFeSi-Particles in Commercial Pure Aluminum," *Zeitschrift fur Metallkunde,* vol. 75, pp. 170-174, 1984.

[45] A. L. Dons, "Variations in the composition of AlMnFeSi-particles in aluminum," *Scandinavian Journal of Metallurgy,* vol. 13, pp. 137-143, 1984.

[46] A. L. Dons, “Superstructures in alpha-Al (Mn, Fe, Cr) Si,” *ZEITSCHRIFT FUR METALLKUNDE,* vol. 76, pp. 151-153, 1985.

[47] H. Westengen, “FORMATION OF INTERMETALLIC COMPOUNDS DURING DC-CASTING OF A COMMERCIAL PURITY AL-FE-SI ALLOY,” *Zeitschrift fur Metallkunde,* vol. 73, pp. 360-368, 1982.

[48] M. Cooper, “The crystal structure of the ternary alloy α (AlFeSi),” *Acta Crystallographica,* vol. 23, pp. 1106-1107, 1967.

[49] E. Nes, S. Naess, and R. Hoier, “Decomposition of an aluminum-manganese alloy,” *Zeitschrift fur Metallkunde,* vol. 63, pp. 248-252, 1972.

[50] H. Hirasawa, “Precipitation process of Al Mn and Al Cr supersaturated solid solution in presence of age hardening phases,” *Scripta Metallurgica,* vol. 9, pp. 955-958, 1975.

[51] L. Lodgaard, and N. Ryum, “Precipitation of dispersoids containing Mn and/or Cr in Al–Mg–Si alloys,” *Materials Science and Engineering: A,* vol. 283, pp. 144-152, 2000.

[52] J. Tian, K. Do Woo, K. J. Lee *et al.*, “Effect of Step Quenching and Zr Addition on the Microstructure and Mechanical Properties of Al-Mg-Si Alloy,” *Korean Journal of Metals and Materials,*vol. 52, pp. 101-111, 2014.

[53] O. Engler, E. Sachot, J. Ehrström *et al.*, “Recrystallisation and texture in hot deformed aluminium alloy 7010 thick plates,” *Materials science and technology,* vol. 12, pp. 717-729, 1996.

[54] H. Yoshida, and Y. Baba, “The role of zirconium to improve strength and stress-corrosion resistance of Al–Zn–Mg and Al–Zn–Mg–Cu alloys,” *Transactions of the Japan Institute of Metals,* vol. 23, pp. 620-630, 1982.

[55] Z. Jia, G. Hu, B. Forbord *et al.*, “Enhancement of recrystallization resistance of Al–Zr–Mn by two-step precipitation annealing,” *Materials Science and Engineering: A,* vol. 483, pp. 195-198, 2008.

[56] X.-y. LÜ, E.-j. Guo, P. Rometsch *et al.*, “Effect of one-step and two-step homogenization treatments on distribution of Al_3Zr dispersoids in commercial AA7150 aluminium alloy,” *Transactions of Nonferrous Metals Society of China*, vol. 22, pp. 2645-2651, 2012.

[57] Z. Guo, G. Zhao, and X.-G. Chen, “Effects of two-step homogenization on precipitation behavior of Al_3Zr dispersoids and recrystallization resistance in 7150 aluminum alloy,” *Materials Characterization,* vol. 102, pp. 122-130, 2015.

[58] V. Ocenasek, and M. Slamova, “Resistance to recrystallization due to Sc and Zr addition to Al–Mg alloys,” *Materials Characterization,* vol. 47, pp. 157-162, 2001.

[59] K. E. Knipling, D. N. Seidman, and D. C. Dunand, “Ambient-and high-temperature mechanical properties of isochronally aged Al–0.06 Sc, Al–0.06 Zr and Al–0.06 Sc–0.06 Zr (at.%) alloys,” *Acta Materialia,* vol. 59, pp. 943-954, 2011.

[60] Z.-h. Jia, J. Røyset, J. K. Solberg *et al.*, "Formation of precipitates and recrystallization resistance in Al–Sc–Zr alloys," *Transactions of Nonferrous Metals Society of China,* vol. 22, pp. 1866-1871, 2012.

[61] Z. Yin, Q. Pan, Y. Zhang *et al.*, "Effect of minor Sc and Zr on the microstructure and mechanical properties of Al–Mg based alloys," *Materials Science and Engineering: A,* vol. 280, pp. 151-155, 2000.

[62] N. Ryum, "Precipitation and recrystallization in an A1-0.5 WT.% Zr-alloy," *Acta Metallurgica,* vol. 17, pp. 269-278, 1969.

[63] O. Izumi, and D. Oelschägel, "On the decomposition of a highly supersaturated Al Zr solid solution," *Scripta Metallurgica,* vol. 3, pp. 619-621, 1969.

[64] E. Nes, "Precipitation of the metastable cubic Al_3Zr-phase in subperitectic Al-Zr alloys," *Acta Metallurgica,* vol. 20, pp. 499-506, 1972.

[65] Z. A. Chaudhury, and C. Suryanarayana, "A TEM study of decomposition behavior of a melt-quenched Al-Zr alloy," *Metallography,* vol. 17, pp. 231-252, 1984.

[66] K. E. Knipling, D. C. Dunand, and D. N. Seidman, "Precipitation evolution in Al–Zr and Al–Zr–Ti alloys during isothermal aging at 375–425°C," *Acta Materialia,* vol. 56, pp. 114-127, 2008.

[67] K. E. Knipling, D. C. Dunand, and D. N. Seidman, "Precipitation evolution in Al–Zr and Al–Zr–Ti alloys during aging at 450–600°C," *Acta Materialia,* vol. 56, pp. 1182-1195, 2008.

[68] K. E. Knipling, D. C. Dunand, and D. N. Seidman, "Nucleation and Precipitation Strengthening in Dilute Al-Ti and Al-Zr Alloys," *Metallurgical and Materials Transactions A,* vol. 38, pp. 2552-2563, 2007.

[69] Z. Jia, G. Hu, B. Forbord *et al.*, "Effect of homogenization and alloying elements on recrystallization resistance of Al–Zr–Mn alloys," *Materials Science and Engineering: A,* vol. 444, pp. 284-290, 2007.

[70] J. D. Robson, and P. B. Prangnell, "Dispersoid precipitation and process modelling in zirconium containing commercial aluminium alloys," *Acta Materialia,* vol. 49, pp. 599-613, 2001.

[71] Z.-h. Jia, J.-P. CouziniÉ, N. Cherdoudi *et al.*, "Precipitation behaviour of Al3Zr precipitate in Al–Cu–Zr and Al–Cu–Zr–Ti–V alloys," *Transactions of Nonferrous Metals Society of China,* vol. 22, pp. 1860-1865, 2012.

[72] D. Tsivoulas, J. D. Robson, C. Sigli *et al.*, "Interactions between zirconium and manganese dispersoid-forming elements on their combined addition in Al–Cu–Li alloys," *Acta Materialia,* vol. 60, pp. 5245-5259, 2012.

[73] P. Vermaut, and P. Ruterana, "A TEM study of a copper rich phase grown on an Al_3Zr dispersoid in a spray formed AlSiC composite," *Acta Materialia,* vol. 44, pp. 2445-2455, 1996.

[74] R. Kaibyshev, F. Musin, D. R. Lesuer *et al.*, "Superplastic behavior of an Al–Mg alloy at elevated temperatures," *Materials Science and Engineering: A,* vol. 342, pp. 169-177, 2003.

[75] B. Forbord, H. Hallem, N. Ryum *et al.*, “Precipitation and recrystallisation in Al–Mn–Zr with and without Sc,” *Materials Science and Engineering: A,* vol. 387-389, pp. 936-939, 2004.

[76] J. D. Robson, “A new model for prediction of dispersoid precipitation in aluminium alloys containing zirconium and scandium,” *Acta Materialia,* vol. 52, pp. 1409-1421, 2004.

[77] Y. Riddle, H. Hallem, and N. Ryum, "Highly Recrystallization Resistant Al-Mn-Mg Alloys Using Sc and Zr." *Trans tech publ,* vol. 396, pp. 563-568, 2002.

[78] Y. Wang, Q.-l. Pan, Y.-f. Song *et al.*, “Recrystallization of Al-5.8Mg-Mn-Sc-Zr alloy,” *Transactions of Nonferrous Metals Society of China,* vol. 23, pp. 3235-3241, 2013.

[79] Y. Meng, Z.-h. Zhao, and J.-z. Cui, “Effect of minor Zr and Sc on microstructures and mechanical properties of Al–Mg–Si–Cu–Cr–V alloys,” *Transactions of Nonferrous Metals Society of China,* vol. 23, pp. 1882-1889, 2013.

[80] W. Lefebvre, F. Danoix, H. Hallem *et al.*, “Precipitation kinetic of Al_3(Sc, Zr) dispersoids in aluminium,” *Journal of Alloys and Compounds,* vol. 470, pp. 107-110, 2009.

[81] B. Forbord, W. Lefebvre, F. Danoix *et al.*, “Three dimensional atom probe investigation on the formation of Al_3(Sc,Zr)-dispersoids in aluminium alloys,” *Scripta Materialia,* vol. 51, pp. 333-337, 2004.

[82] E. Clouet, L. Laé, T. Épicier *et al.*, "Complex precipitation pathways in multicomponent alloys," *Nature materials,* vol. 5, pp. 482, 2006.

[83] Z.-h. Jia, J. RØYset, J. K. Solberg *et al.*, "Formation of precipitates and recrystallization resistance in Al–Sc–Zr alloys," *Transactions of Nonferrous Metals Society of China,* vol. 22, pp. 1866-1871, 2012.

[84] C. B. Fuller, D. N. Seidman, and D. C. Dunand, "Mechanical properties of Al(Sc,Zr) alloys at ambient and elevated temperatures," *Acta Materialia,* vol. 51, pp. 4803-4814, 2003.

[85] F. Musin, R. Kaibyshev, Y. Motohashi *et al.*, "High strain rate superplasticity in a commercial Al–Mg–Sc alloy," *Scripta Materialia,* vol. 50, pp. 511-516, 2004.

[86] J.-H. Xu, and A. Freeman, "Phase stability and electronic structure of $ScAl_3$ and $ZrAl_3$ and of Sc-stabilized cubic $ZrAl_3$ precipitates," *Physical Review B,* vol. 41, pp. 12553, 1990.

[87] M. Conserva, and M. Leoni, "Effect of thermal and thermo-mechanical processing on the properties of Al-Mg alloys," *Metallurgical Transactions A,* vol. 6, pp. 189-195, 1975.

[88] S. W. Cheong, and H. Weiland, "Understanding a microstructure using GOS (grain orientation spread) and its application to recrystallization study of hot deformed Al-Cu-Mg alloys," *Materials Science Forum,* vol. 558, pp. 153-158, 2007.

[89] M. J. Starink, N. Gao, N. Kamp *et al.*, "Relations between microstructure, precipitation, age-formability and damage tolerance of Al–Cu–Mg–Li (Mn, Zr, Sc) alloys for age forming," *Materials Science and Engineering: A*, vol. 418, pp. 241-249, 2006.

[90] T. Ohashi, L. Dai, and N. Fukatsu, "Decomposition characteristics of Al-Mn-Zr alloys rapidly-quenched from the melt," *Metallurgical Transactions A*, vol. 17, pp. 799-806, 1986.

[91] B. Forbord, L. Auran, W. Lefebvre *et al.*, "Rapid precipitation of dispersoids during extrusion of an Al–0.91wt.% Mn–0.13wt.% Zr–0.17wt.% Sc-alloy," *Materials Science and Engineering: A*, vol. 424, pp. 174-180, 2006.

[92] B. Forbord, H. Hallem, and K. Marthinsen, "ICAA-9: 9th international conference on aluminium alloys," *Brisbane, Australia*, pp. 1179-1185, 2004.

[93] A. B. Johansen, O, and J. R. Embury, N, "Alloy development in the Al-Mg-alloy system, Part I," *Aluminium-Dusseldorf*, vol. 82, pp. 980-985, 2006.

[94] D. Tsivoulas, and J. D. Robson, "Heterogeneous Zr solute segregation and Al_3Zr dispersoid distributions in Al–Cu–Li alloys," *Acta Materialia*, vol. 93, pp. 73-86, 2015.

[95] M. Peters, J. Eschweiler, and K. Welpmann, "Strength profile in Al Li plate material," *Scripta metallurgica*, vol. 20, pp. 259-264, 1986.

[96] J. Robson, “Microstructural evolution in aluminium alloy 7050 during processing,” *Materials Science and Engineering: A,* vol. 382, pp. 112-121, 2004.

[97] L. E. Murr, “Interfacial phenomena in metals and alloys,” *Addison-Westly Publ,* pp. 387, 1975.

CHAPTER 3

EXPERIMENTAL PROCEDURES

3.1 Alloy preparation

In the present work, alloys with different contents of Mn, Zr and Sc additions were designed in the present study. The composition assigned to alloy-A, alloy-B, alloy-C, alloy-D and alloy-E were listed in Table. 3.1. Approximately 3 kilograms of materials for each composition were batched in an electrical resistance furnace and then cast in the permanent mold as a rectangular billet (30 mm*40 mm*80 mm).

Table 3.1: Chemical composition (in wt.%) of designed AA6082 alloys.

Alloy	Mg	Si	Fe	Mn	Zr	Sc	Al
A	1.0	0.7	0.3	-	-	-	Bal.
B	1.0	0.7	0.3	0.5	-	-	Bal.
C	1.0	0.7	0.3	1.0	-	-	Bal.
D	1.0	0.7	0.3	1.0	0.2	-	Bal.
E	1.0	0.7	0.3	1.0	0.1	0.1	Bal.

Accordingly, one condition (400℃/2h) was selected as the pre-deforamtion heat treatment for the following hot rolling. The pre-heat treated samples were firstly cut into cubes with size of 30 mm*40 mm*40 mm, preheated to 400 ℃ for 30 minutes and then subjected to the hot rolling at 400 ℃ into a thickness of 3 mm from original

30 mm. The indenting displacement was controlled at 3 mm for each pass. A schematic of the rolling and transverse direction was shown in Fig. 3.1.

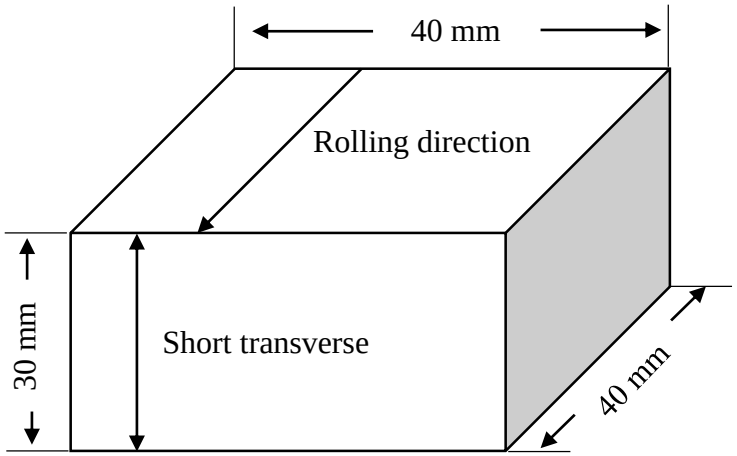

Fig. 3.1 The schematic of the samples to be rolled.

3.2 Heat treatment

As-cast billets were subjected to various heat treatment temperatures ranging from 300-500 ℃ for up to 24 hours with a heating rate of 100 ℃/h, followed by water quenching.

For the annealing process, the as-rolled samples were heated rapidly to 500 ℃ for 1, 2, 4 and 8 hours, followed by water quenching, as shown in Fig. 3.2.

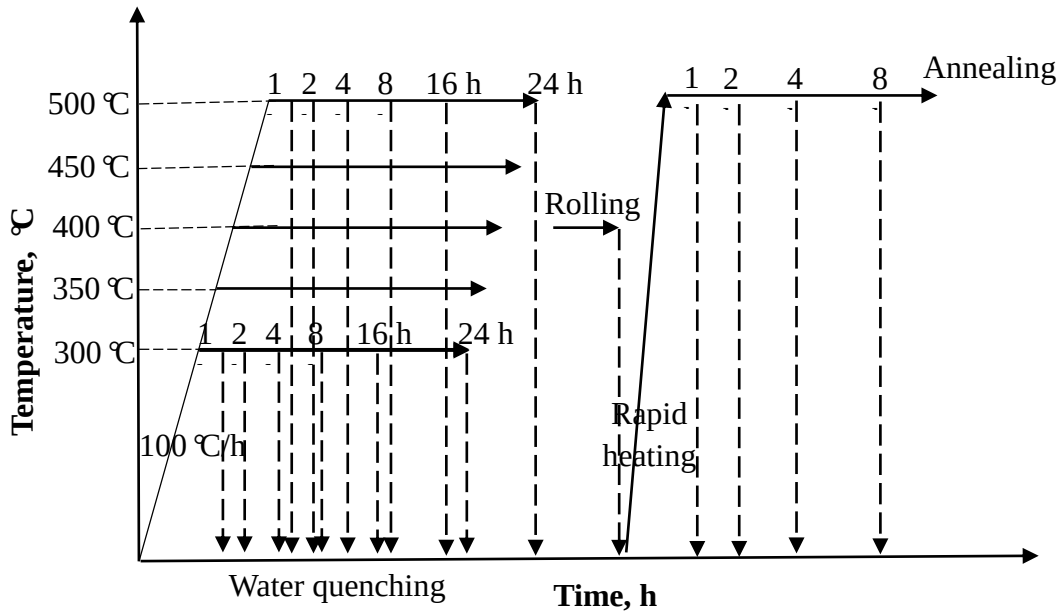

Fig. 3.2 Heat treatment parameters of the designed alloys.

3.3 Materials Characterization

3.3.1 Morphology observation

Microstructures, especially the distribution of dispersoids subjected to various heat treatments, were characterized under an optical microscope (OM), a scanning electron microscope (SEM, JOEL JSM-6480LV) operated at 15kV and transmission electron microscope (TEM, JEOL JEM-2100) operated at 200kV respectively. OM and SEM specimens were cross-sectioned into small slices with thickness of 3mm, mounted into graphite cylinder and polished afterwards with 0.5 μm SiC suspension as the final step. Before observation, all of the samples were etched into 0.5% HF solution for 25 s. TEM specimens were mechanically grounded to approximately 40 μm, followed by twin-jet eletropolishing at 15V DC in a 30% nitric acid and 70% methanol solution cooled to -20 ℃. The samples were observed in dark field through the <001> plane of Al matrix to reveal $L1_2$ Al_3Zr and $Al_3(Sc,Zr)$ dipsersoids.

Morphology of hot-rolled samples before and after annealing was also characterized in the present study. To quantify the recrystallized structure, all as-rolled and annealed specimens were sectioned parallel to the rolling direction and polished, then mapped using the electron backscattered diffraction (EBSD) technique on the SEM. Three different areas of 0.24 mm^2 for each condition were scanned with a step size of 2 μm.

The recrystallized grains were determined based on EBSD images by the following criteria:

1. The recrystallized grains were separated by high angle boundaries (>15 °) from the unrecrystallized grains.
2. No relatively large integral substructures surrounded by low angle boundaries (2-15 °) existed in the recrystallized grains.

TEM specimens of as-rolled and annealed samples were mechanically grounded to approximately 40 μm along with the rolling direction, followed by the same procedure as that of the casting specimens. The samples were observed through the [011] zone axis of Al matrix in order to see both distribution of dispersoids and dislocations.

3.3.2 Image analysis

The size, number density and area percentage of dispersoids was all obtained directly based on SEM and TEM images through Clemex image analysis software. In order to calculate the pinning force induced by the dispersoids, local volume fraction of dispersoids in the dispersoid zone rather than the average volume fraction was employed, since the pinning force in the dispersoid zone can better reflect the overall resistance to the recrystallization compared with the average pinning force for the

facts that regions in dispersoid free zones where no pinning force resulted from dispersoids existed are actually supposed to recrystallize very quickly and only regions in dispersoid zones can effectively resist the recrystallization process. Besides, dispersoid zones occupied ~ 90% area percentage for the selected conditions in the present study, which means as long as the pinning force in the dispersoid zones is high enough to resist the recrystallization, it will be suppressed efficiently. To quantify the local volume fraction of dispersoids, dispersoids were simulated to be spherical and the local volume fraction was given by the following equation:

$$F_v = A_A \frac{2D}{3t} \tag{3.1}$$

Where, D is the equivalent diameter of dispersoids, A_A is the area percentage of dispersoids from TEM observation, t is the thickness of the observed area which was determined by electron energy loss spectroscopy (EELS) equipped in TEM. More than 200 particles were analyzed to secure the accuracy of the results.

3.3.3 Mechanical properties

In order to evaluate the evolution of dispersoids during heat treatments and their influence on properties at room temperature (RT), electrical conductivity (EC) and Vickers micro-hardness measurements were conducted on the heat treated alloys. EC

was measured using a Sigmascope SMP10 electrical conductivity unit at RT and the average value of 3 measurements was recorded for each sample. Micro-hardness tests were performed on a NG-1000 CCD microhardness test machine with a load of 10 g and a dwell time of 20 s on polished samples. The indentations were pressed in the dendrite cell to evaluate the strengthening effect of dispersoids. More than 15 measurements were performed on each sample.

The elevated-temperature YS were obtained from compression tests performed on a Gleeble 3800 machine at 300 ℃ with a total strain of 0.2 and a fixed strain rate at 10^{-3} s^{-1}. The specimens were machined to small cylinders as shown in Fig. 3.3 from the casting billets and subjected to the various heat treatments ranging from 350-450 ℃ as mentioned before. To eliminate strengthening effect induced by Mg, Si solutes and precipitates, samples were all hold at 300 ℃ for 100 hours before the compression tests.

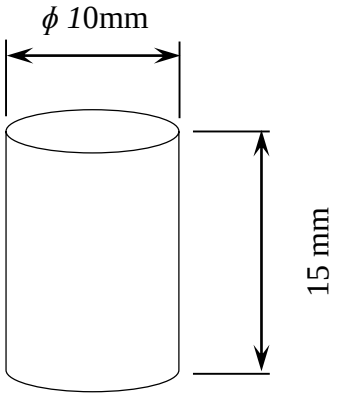

Fig. 3.3 Specimen dimension for the compression tests.

CHAPTER 4

EFFECT OF MN CONTENT AND HEAT TREATMENTS ON DISPERSOIDS AND RECRYSTALLIZATION RESISTANCE

In this chapter, Al-Mg-Si 6082 type alloys containing different Mn additions were subjected to various heat treatments ranging from 300-500 ℃ for different soaking times. After that, the annealing process at 500 ℃ after hot-rolling was performed. The investigation was initiated with figuring out the evolution of dispersoids during the heat treatments aiming to discover the optimum heat treatment parameters, under which dispersoids with finer size and larger density could be obtained and relatively higher elevated-temperature property could be achieved. Further attention was paid to recrystallization behaviors during the annealing process followed hot-rolling. The influence from the evolution of dispersoids during annealing on recrystallization was quantitatively analyzed.

4.1 Evolution of dispersoids during heat treatments with various Mn contents

According to literature [1], the EC of the experimental alloys has the relationship with the concentrations of the alloying elements in the solid solution as follows:

$$1/EC_{Alloy\text{-}A}=0.0267+ 0.032\ Fe_{ss}\%+0.0068Si_{ss}\% + 0.003Mg_{ss}\% \quad (4.1)$$

$$1/EC_{Alloy\text{-}B/C}=0.0267+ 0.032\ Fe_{ss}\%+ \mathbf{0.033Mn_{ss}\%}+ 0.0068Si_{ss}\% + 0.003Mg_{ss}\% \quad (4.2)$$

Where, $Fe_{ss}\%$, $Mn_{ss}\%$, $Si_{ss}\%$ and $Mg_{ss}\%$ are the weight percentages of the solute elements Fe, Mn, Si and Mg. It can be found that Si_{ss} and Mg_{ss} have much less effect on EC than Mn_{ss} and Fe_{ss}, and most of Fe was in the form of intermetallics during solidification, such as $Al_6(MnFe)$ and α-Al(MnFe)Si [2]. Therefore, the change on the EC difference between Alloy-B/C and Alloy-A can be used to estimate the evolution of Mn solid solution concentration in Alloy-B/C during heat treatment by:

$$1/EC_{Alloy\text{-}B/C} - 1/EC_{Alloy\text{-}A} = \Delta\rho = 0.033Mn_{ss}\% \quad (4.3)$$

Fig.1 shows the differences in 1/EC (Δρ) between Alloy-B/C and Alloy-A with temperature and holding time of heat treatments. Similar tendency was found on Δρ between Alloy-B and Alloy-A (Fig. 4.1a) as well as between Alloy-C and Alloy-A

(Fig. 4.1b). When heat-treated at 300 ℃, Δρ was high but relatively stable with soaking time, which can be attributed to the likely reason that most of the solute Mn atoms are still remaining in the aluminum matrix in Alloy B/C. At 350 ℃, Δρ started deviating from the difference line at 300 ℃ and decreased sharply with increasing holding time, indicating the decreasing Mn solute concentration in the matrix and the formation of dispersoids. Variation of Δρ at 400 ℃ and 450 ℃ were similar, which exhibited an initial fast drop followed by a plateau after 8 hours' holding, indicating the fully decomposition of Mn supersaturate solid solution. Δρ at 500 ℃ showed the lowest value among the given heat treatment conditions and paralleled with the plateau achieved at 400 ℃ and 450 ℃, suggesting that decomposition of Mn solutes in the solid solution was completed before 1 hour's holing at 500 ℃. Therefore, the most important range for the formation and evolution of dispersoids is 350-500 ℃.

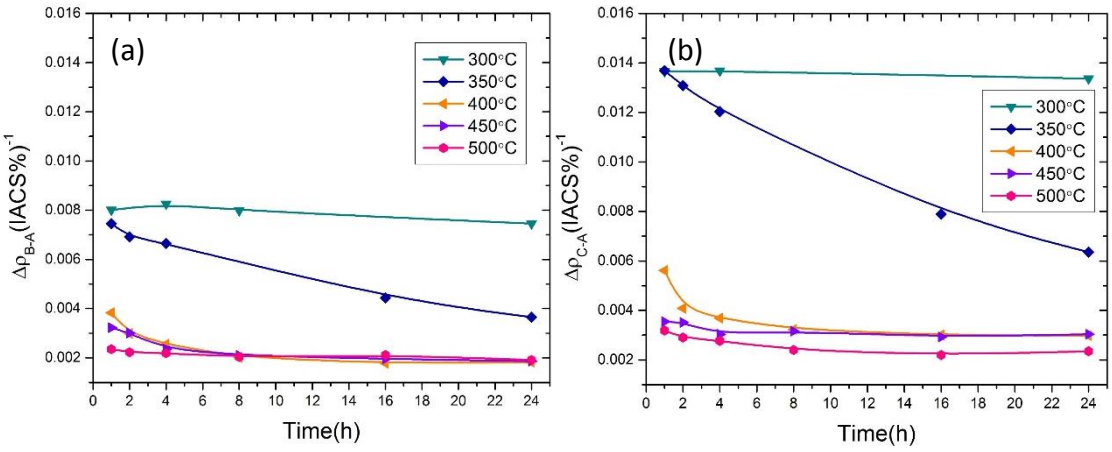

Fig. 4.1 Difference in 1/EC: (a) between Alloy-B and Alloy-A and (b) between Alloy-C and Alloy-A.

Therefore, the difference in Vickers microhardness (ΔHV) between Alloy-B/C and Alloy-A in the temperature range of 350-500 ℃ is shown in Fig. 4.2. Generally, the curves can be categorized into two types in both Fig. 4.2a and 2b: type Ⅰ is in the range of 350 ℃~400 ℃, where the ΔHV keeps increasing until to plateau while it begins to drop after the peak at 450 ℃~500 ℃ (type Ⅱ), indicating the various influence of heat treatment temperatures on the properties. As shown in Fig. 4.2, ΔHV shows the highest value at 400 ℃, which is 20 HV for ΔHV_{B-A} and 25 HV for ΔHV_{C-A}. Meanwhile, compared with ΔHV_{B-A} in Fig. 4.2a, the ΔHV_{C-A} in Fig. 4.2b is generally 5-10 HV higher until to 500 ℃ at which similar even lower value is observed for ΔHV_{C-A}, showing the various effect of Mn additions during heat treatments. Since the changes of hardness are greatly related to the evolution of dispersoids and the two types from Fig. 4.2, the evolution of dispersoids during the heat treatment at 400 ℃(type Ⅰ) and 500 ℃ (type Ⅱ) was selected for detailed discussed in the following sections.

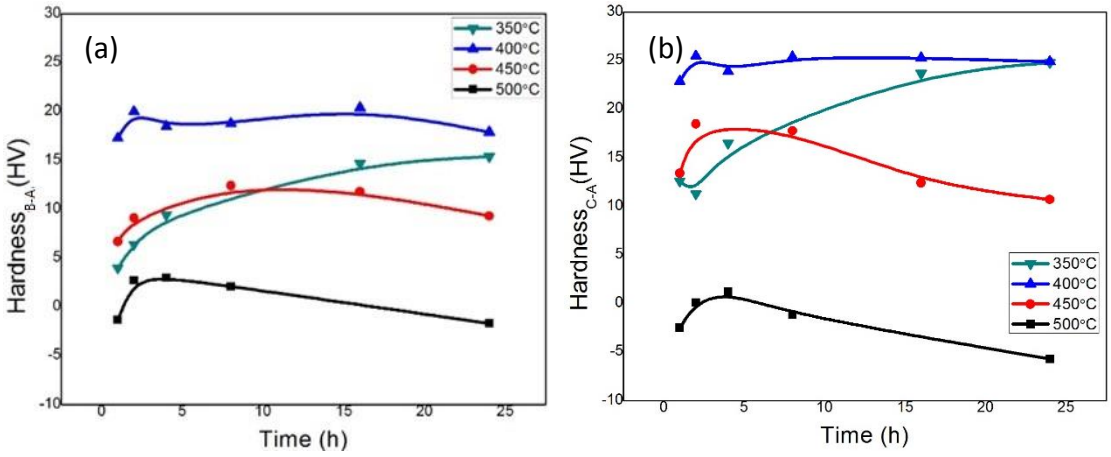

Fig. 4.2 Differences in Vickers hardness (ΔHV) between (a) Alloy-B and Alloy-A and (b) Alloy-C and Alloy-A as a function of heat treatment time and temperature.

Fig. 4.3 shows the SEM images revealing the distribution of dispersoids at heat treatment temperature of 400 ℃. In Alloy-A, no dispersoids could be observed even after 24 hours at 400 ℃ (Fig. 4.3a). However, in Alloy-B (Fig. 4.3b-d) and Alloy C (Fig. 4.3 e-g), fine dispersoids were already uniformly distributed in the matrix after 1 hour's holding at 400 ℃ and no evident distinctions could be observed even after soaking at 400 ℃ for 24 hours. This is in line with the quantitative results in Fig. 4.4, showing that the size of dispersoids remained fine up to 24 hours with a diameter of ~ 74 nm in Alloy-B and ~ 85 nm in Alloy-C, while the number density initially increased over the first 2 hours and then remained steady. The above results indicated that the dispersoids are starting to precipitate below 400 ℃, such as 350 ℃ in Figs. 1 and 2 with decreasing EC and increasing ΔHV, and they reached to the optimum and stable condition after 2 h at 400 ℃. Therefore, the higher volume of finer dispersoids leads to the highest ΔHV at 400 ℃ (Fig. 4.2). On the other hand,

differences can be observed between Alloy B and Alloy C by comparing Figs. 3b-d and e-g. A much denser distribution of dispersoids was observed in Alloy-C than in Alloy-B after heat treated at 400 ℃ for 1 hour and this larger density was still quite obvious even after 24 hours, while the dispersoid size in Alloy-C was close to that in Alloy-B. As shown in Fig. 4.4, the number density of dispersoids after 24 h at 400 ℃ increased from ~9 μm^{-2} in Alloy-B to ~13 μm^{-2} in Alloy-C, while the equivalent diameter only slightly increased from ~74 nm for Alloy-B to ~85 nm in Alloy-C. Therefore, further addition of Mn could increase the volume of dispersoids without sacrificing the size when treated at the lower temperatures (350-400 ℃), during which the nucleation and growth dominated the precipitation behavior of dispersoids.

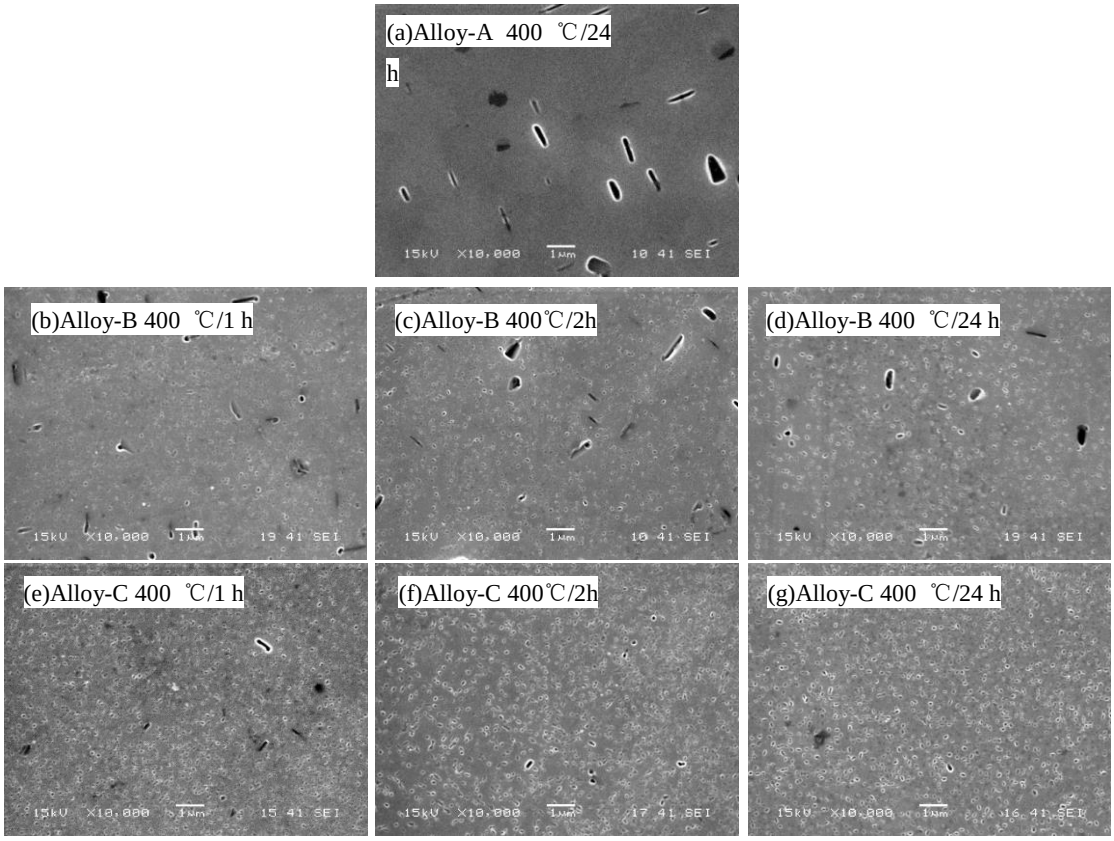

Fig. 4.3 SEM images of (a) Alloy-A after heat treatment at 400 ℃ for 24 hours, (b-d) Alloy-B and (e-g) Alloy-C after heat treatment at 400 ℃ for 1 hour, 2 hours and 24 hours respectively.

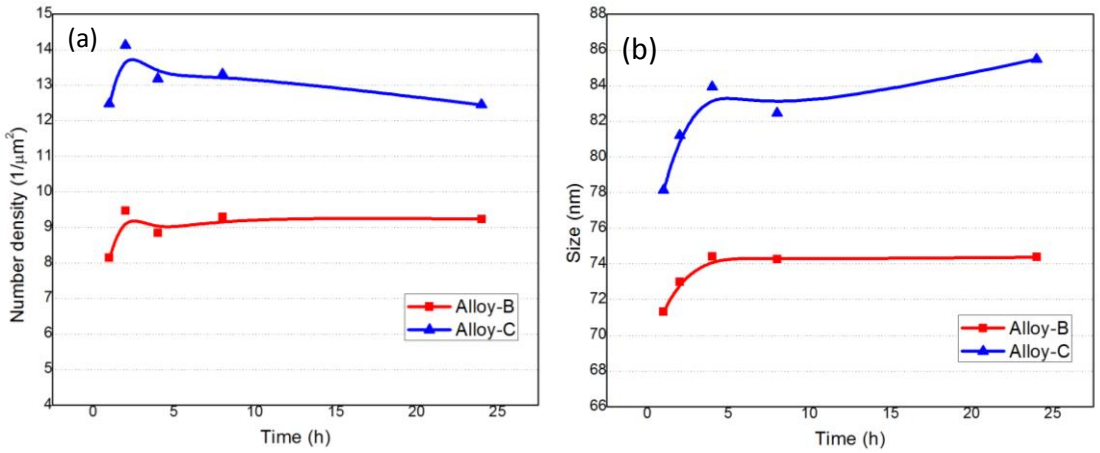

Fig. 4.4 (a) Number density and (b) equivalent diameter of dispersoids as a function of holding time at heat treatment temperature of 400 ℃.

In addition, Fig. 4.5 presents the evolution of dispersoids in Alloys B and C at 500 ℃. Comparing Figs. 4.5a-b with Figs. 3b and d as well as the Figs. 4.5c-d to Figs. 4.3e and g, it is apparent that size of dispersoids at 500 ℃ after 1 hour was much larger than that at 400 ℃ and still became larger after 24 hours while the density keep decreasing, indicating that the coarsening of dispersoids dominated the precipitation behaviors of dispersoids at 500 ℃, which resulted in the lowest ΔHV at 500 ℃ for both Alloy-B and Alloy-C (Fig. 4.2). As shown in Fig. 4.6, the size of dispersoids at 500℃/24h is already reached to 105 and 145 nm with the number density decreases to 2 and 3.5 μm^{-2} in Alloys B and C, respectively, which was greatly different with that at 400 ℃ in Fig. 4.4 (74 and 85 nm as well as 9 and 12.5 μm^{-2}).

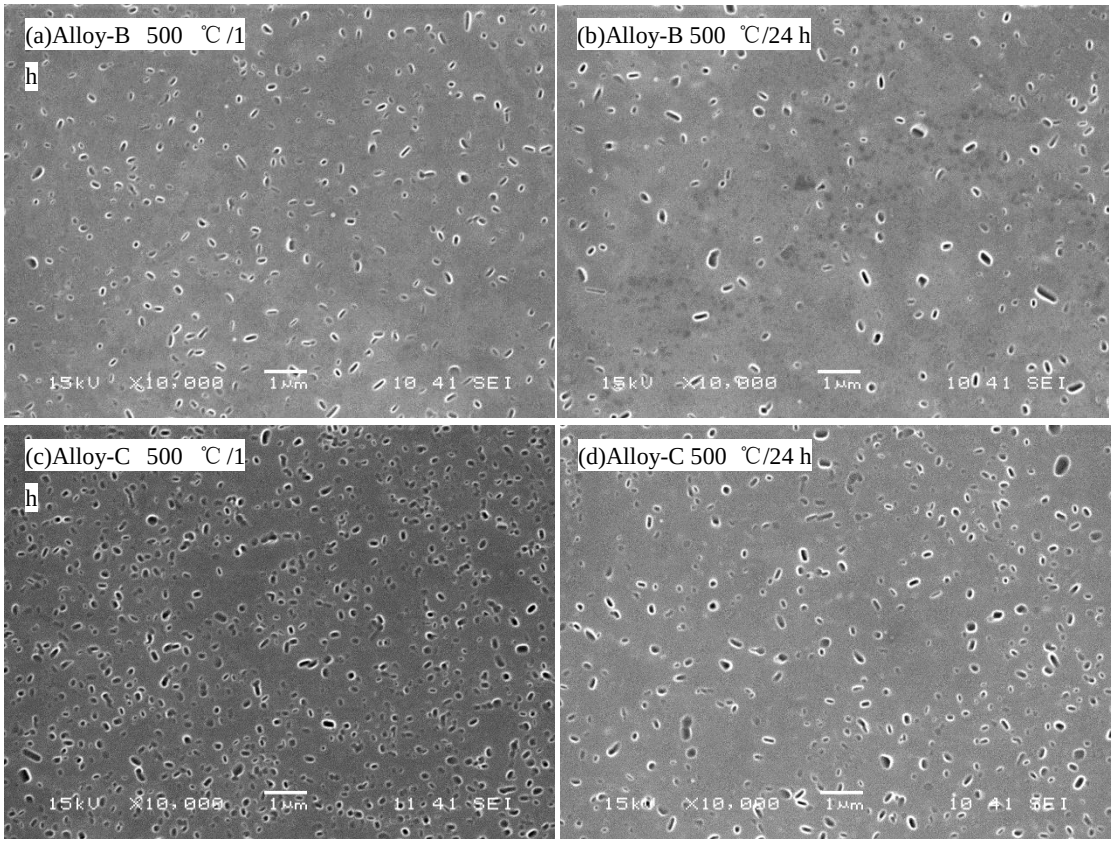

Fig. 4.5 SEM images of (a,b) Alloy-B and (c,d) Alloy-C after heat treatment at 500 ℃ for 1 hour and 24 hours respectively.

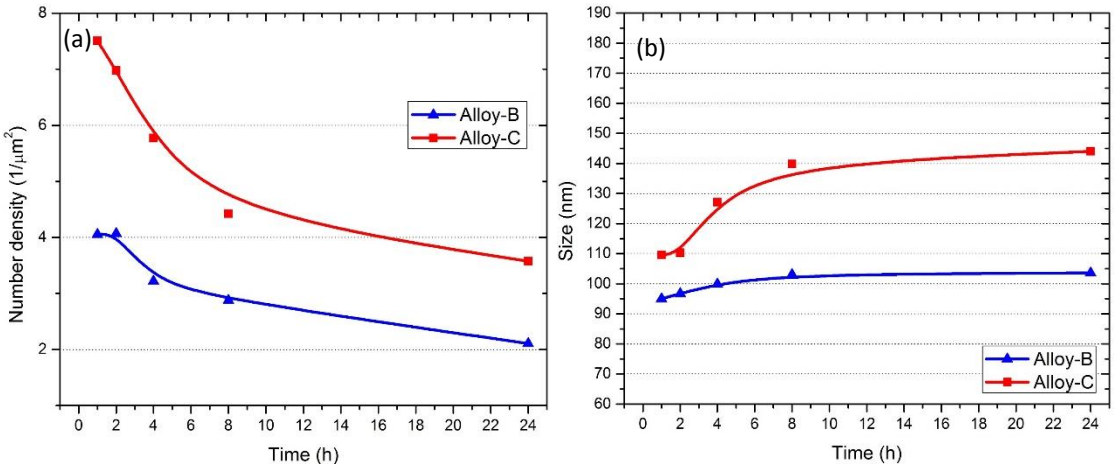

Fig. 4.6 (a) Number density and (b) equivalent diameter of dispersoids as a function of holding time at heat treatment temperature of 500 ℃.

Meanwhile, differences between Alloy B and Alloy C can also be observed. As shown in Fig. 4.5c at 500℃/1h, the size of dispersoids is similar with Alloy B (Fig. 4.5a) but with higher number density. However, the coarsening rate is higher in Alloy C than Alloy B with increasing holding time. As shown in Fig. 4.5d, the size of dispersoids is much bigger than Fig. 4.5b while the number density is similar. As shown in Fig. 4.6, the equivalent diameter of dispersoids in Alloy-C coarsened much faster, from 109.58 to 144.02 nm for Alloy-C in comparison with from 95 to 103.6 nm and the number density of dispersoids in Alloy-C dropped more sharply than that in Alloy-B, from 7.5 to 3.5 μm^{-2} for Alloy-C compared with from 4.1 to 2.1 μm^{-2} for Alloy-B. Therefore, at high temperature range (450-500 ℃) during which coarsening was the main mechanism, excessive Mn addition could promote the coarsening process by accelerating the declination in number density and growth in size of dispersoids.

These various influence of heat treatments and Mn contents on dispersoids during different temperature ranges can be attributed to the rapid increase of diffusion rate of Mn element with increasing temperature [3]. At a relatively lower temperature, the diffusion of Mn solutes was limited in small regions, thus the growth of dispersoids was inhibited. Whereas at high temperature ranges, long distance diffusion of Mn solutes became available and then the coarsening of dispersoids is promoted. On the other hand, higher Mn content resulted into the shorter distance between Mn solutes which simplified the Mn diffusion from Mn rich region to the interface of Mn-containing dispersoids. Meanwhile, the excessive addition of Mn hugely increased the concentration gradient at the interface of dispersoids, the influence of which on diffusion rate was mitigated by a small diffusion coefficient at low temperatures but amplified by a large diffusion coefficient at high temperatures. This led to the distinct effects of Mn contents on dispersoids under various temperature ranges, as shown in Figs. 4.4 and 4.6.

As shown in Figs. 4.3 and 4.5, various behaviors of dispersoids in Alloy-B and Alloy-C can be observed. Therefore, several conditions, including the nucleation/growth stage (350℃/24h), optimum condition (400℃/2h) and coarsening stage (450℃/16h) were selected to measure the Yield strength ($\sigma_{0.2}$) at 300 ℃ and the results are shown in Fig. 4.7. It was evident that a remarkable improvement in $\sigma_{0.2}$ in Alloys B/C containing Mn-dispersoids compared with Alloy-A under all given heat treatment conditions, confirming the significant contribution of Mn-containing

dispersoids on the improvement of elevated-temperature property in experimental 6082 alloys. It can be found the highest $\sigma_{0.2}$ is obtained at 400℃/2h, which is 55 MPa and 70 MPa for Alloys-B and C compared with 30 MPa in Alloy-A. Meanwhile, $\Delta\sigma_{0.2}$ between Alloy-B and Alloy-C is also changing with conditions. At 400℃/2h, $\Delta\sigma_{0.2}$ between Alloy-B and Alloy-C is found to be 15 MPa due to the higher number density of dispersoids but with similar size in Alloy-C than Alloy-B (shown in Fig. 4.3c, 3f and Fig. 4.4). However, the excessive addition of Mn in Alloy-C at higher temperature (450-500 ℃) results in the higher coarsening rate of dispersoids, therefore, the differences in $\Delta\sigma_{0.2}$ decreased to 3.9 MPa at 450℃/16h.

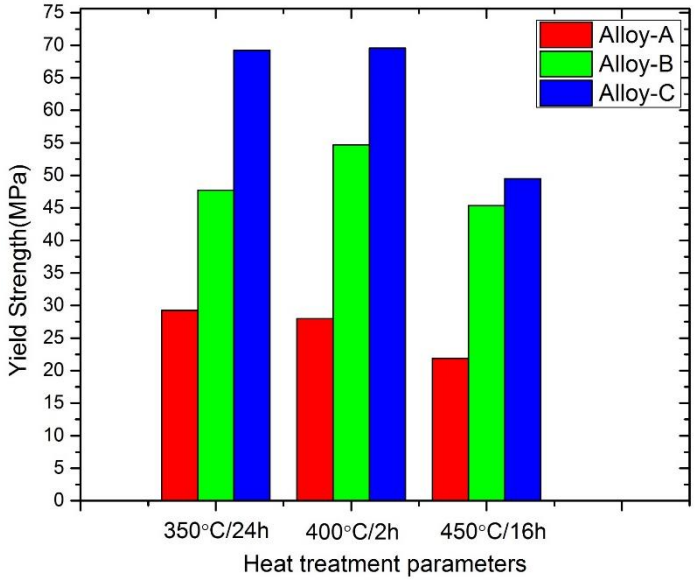

Fig. 4.7 Yield strength of alloys as a function of heat treatment parameters.

4.2 Recrystallization behaviors of experimental alloys

According to the discussion in Section 3.1, 400 ℃ for 2 hours was selected to be the pretreatment before rolling due to its superior condition of dispersoids in size and number density. Typical images of heat treated Alloy-A, Alloy-B and Alloy-C after hot-rolling and subsequent annealing were obtained through EBSD and shown in Fig. 4.8, in which the distinct structures were revealed due to the various Mn contents. In as-rolled condition, Alloy-B and Alloy-C were severely deformed into elongated structures parallel to the rolling direction (Figs. 8b and c), while only peripheral coarse grains separated by high angle boundaries (>15 °) were observed in Alloy-A (Fig. 4.8a). Additionally, the distribution of the grains in Alloy-A remained similar throughout the hot-rolling and subsequent annealing but the peripheral coarse grains containing tangles of low angle boundaries (2-15 °) evolved homogeneously and gradually into more equiaxed grains without low angle boundaries inside, which can be clarified to the continuous recrystallization [4]. However, in Alloy-B and Alloy-C, recrystallized grains nucleated and grew heterogeneously from the boundaries between the elongated bands throughout the post-deformation annealing, and the regions consisting of equiaxed fine grains could be easily distinguished from the regions with elongated deformed bands, which is the typical discontinuous recrystallization behavior [4].

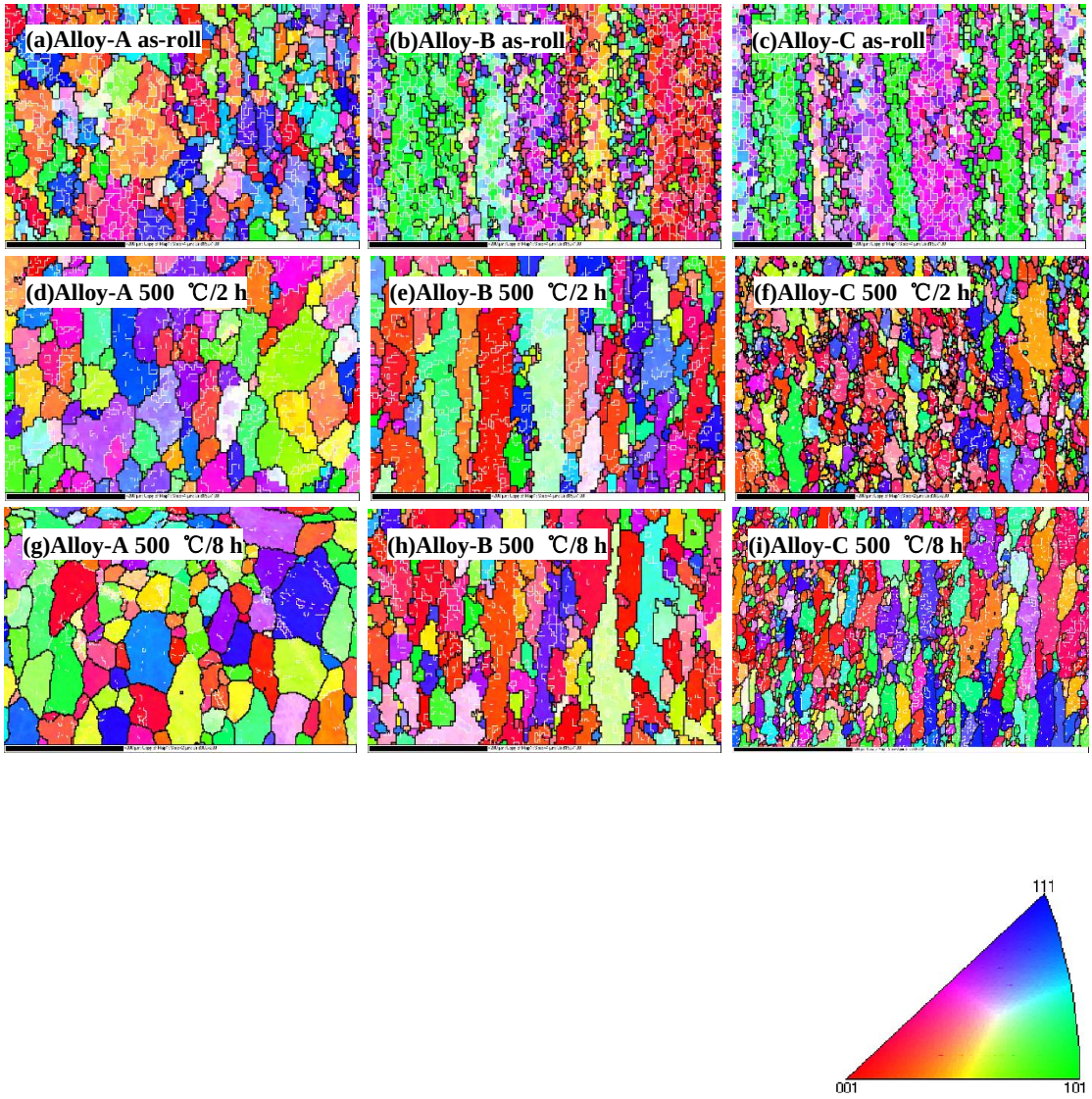

Fig. 4.8 Orientation maps of Alloy A (a, d, c), Alloy B (b, e, h) and Alloy C (c, f, i) following hot rolling and subsequent annealing at 500 ℃ for 2 and 8 hours respectively.

The transformation from continuous recrystallization in Alloy-A to discontinuous recrystallization in Alloys B and C can be attributed to the various microstructures, especially the formation of dispersoids, which was qualitatively explained in Figure. 9. As indicated, after the pre-treated at 400 ℃ for 2 hours, only Mg_2Si sparsely distributed in Alloy-A. While in Alloy-B/C, large quantities of dispersoids also

decomposed homogeneously in the matrix besides Mg_2Si. When they were undergoing the hot deformation, both the Mg_2Si particles and Mn-containing dispersoids could stagnate the rotation of the nearby matrix and thus lead to a regional misorientation with respect to the orientation of the particle-free region. It has been reported in literatures [5] that, the further the distance from the interface of the particle is, the lower the misorientation will be. H. J. Humphreys [25] also indicated in Al-Si system that at a given strain of 0.5, misorientation induced by smaller particles with diameter lower than 1 μm could range from 10° to as large as 35°. Therefore in Alloy-A where large areas of PFZ (indicated by squares) existed among sparsely distributed Mg_2Si precipitates (indicated by circles), a large orientation gradient between particles and the center of PFZ can be expected during deformation. While in Alloys B/C, such orientation gradient can hardly form since particles and dispersoids (indicated by circles) evenly distributed and PFZ only existed in rather small fraction. Associated with the simultaneous occurrence of recovery during the hot deformation, the larger orientation gradient in Alloy-A, which was a significant prerequisite for continuous recrystallization [6], would finally evolve into new high angle boundaries inside original grains, while only low angle boundaries can be formed due to the low orientation gradient in Alloy-B/C,

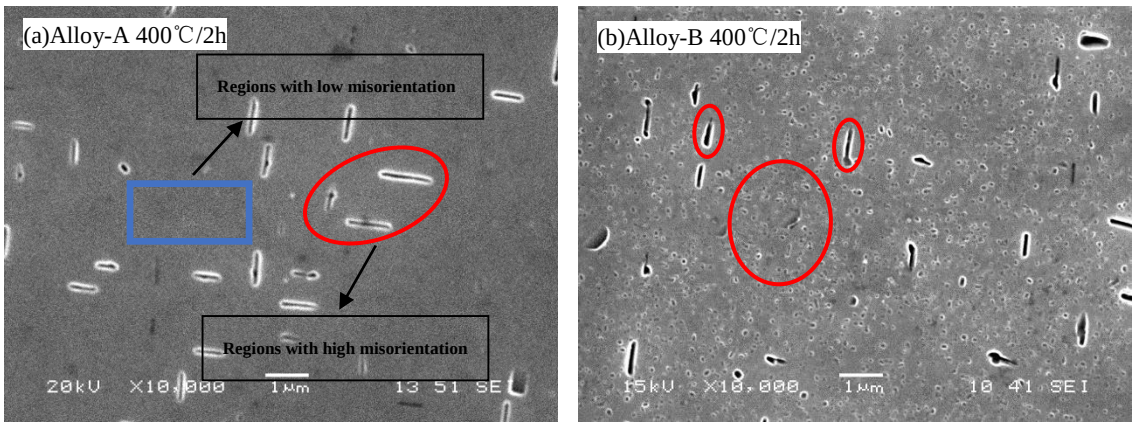

Fig. 4.9 SEM images of (a) Alloy-A and (b) Alloy-B after heat treatment at 400 ℃ for 2 hours.

Fig. 4.10 shows the recrystallization volume fraction (X_v) of experimental alloys after hot-rolling and subsequent annealing. In general, X_v of all the three alloys increased along with the annealing process but it generally smaller in Alloy-C than that of Alloy-A but higher than that of Alloy-B. More details can be revealed combined with Fig. 4.8. In the as-rolled state, all of the three alloys exhibited low content of recrystallization as indicated in Figs. 8a-c that quantities of substructures divided by low angle boundaries existed inside coarse grains of all the three alloys though they were deformed into different shapes. After annealing at 500 ℃ for 2 hours, the gaps between X_v of different alloys started to show up. X_v of Alloy-A increased rapidly from ~10% to ~35% due to the annihilation of low angle boundaries. On the other hand, elongated grains still dominated microstructures in Alloy-B, although equiaxed grains with a little bigger size compared with those in as-rolled Alloy-B evolved from boundaries between the deformed structures, resulting in a very limited growth in X_v of Alloy-B. Alloy-C containing more Mn than Alloy-B, however, exhibited a X_v

between Alloy-A and Alloy-B. As shown in Fig. 4.8f, the former elongated structures broke into much shorter but still elongated grains, severed by several fine equiaxed grains. As annealing time extended from 2 to 8 hours, distribution of high angle boundaries still remained similar but further annihilation of low angle boundaries occurred and no substructures could be observed in more than half of the grains in Alloy-A, resulting in a X_v ~75% in Alloy-A (Fig. 4.8g). While in Alloy-B, the recrystallization process was significantly stagnated, elongated grains still existed in large percentage and no obvious variation in amount of the fine equi-axed grains was observed (Fig. 4.8 h). In Alloy-C shown in Fig. 4.8i, even though the general morphology did not change apparently during annealing process, the quantity of recrystallized fine grains increased with the holding time, leading to a higher X_v than Alloy B. Nevertheless, the inhibition effect of Alloy-C was still superior to that of Alloy-A.

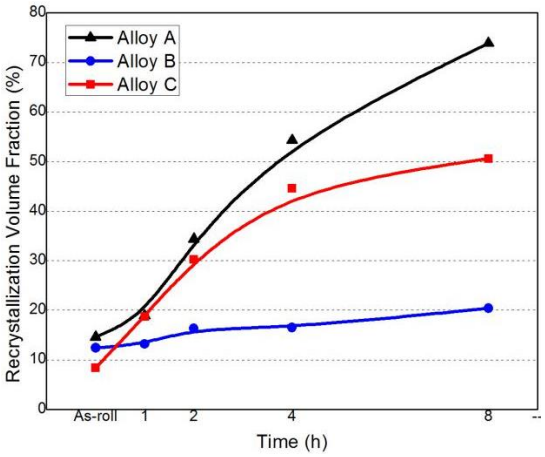

Fig. 4.10 Recrystallization volume fraction of alloys following hot-rolling and subsequent annealing.

As shown in Fig. 4.10, both Alloy-B and C have lower recrystallization volume fraction than Alloy-A, which can be attributed to the Zener drag induced by the existence of large quantities of dispersoids in Alloy-B and C other than Alloy-A, which is in consistence with the literature that formation of dispersoids can greatly improve the recrystallization resistance [7-11]. However, Alloy-C is found to behavior poorer resistance than Alloy-B though more dispersoids with similar size were observed in Alloy-C than in Alloy-B after pre-heat treatment at 400 ℃ for 2 hours (Figs. 3 and 4). Two possible reasons were proposed in the present work for this eccentric phenomenon.

One of the most likely is the evolutions of dispersoids during annealing with different Mn contents. As a result, the distributions of dispersoids in Alloy-B and Alloy-C after hot-rolling and subsequent annealing were exhibited through TEM in Figs. 4.11 and their volume fraction and equivalent diameter are listed in Table. 4.1. As shown in Figs. 4.11a and d, fine and spherical dispersoids were observed being densely distributed in both Alloy-B and Alloy-C after hot-rolling. Meanwhile, as shown in Table 4.1, the equivalent diameters were similar, 36.5 nm for Alloy-B and 46.8 nm for Alloy-C while the volume fraction in Alloy-C was a little larger (2.7 vol.%) than that in Alloy-B (1.8 vol.%). However, different changes on the dispersoids in Alloy-B and C were observed during the annealing. Following the subsequent annealing at 500 ℃ for 1 hour, the size of dispersoids in Alloy-B grew slightly to 44.0 nm, in strong contrast with that in Alloy-C, whose size increased rapidly to 83.6 nm,

suggesting a much higher coarsening rate of dispersoids in Alloy-C than in Alloy-B. With further increasing the annealing time to 8 hours, coarsening phenomena also occurred in Alloy-B, which the size of dispersoids became 86.3 nm compared with 44 nm after 1 hour's annealing. Meanwhile, the dispersoids in Alloy-C keep coarsening to 95.5 nm. Therefore, these different changes of dispersoids must lead to the various pinning force induced by dispersoids, which had strong influence on retarding the recrystallization by effecting both the nucleation and the growth of the grains.

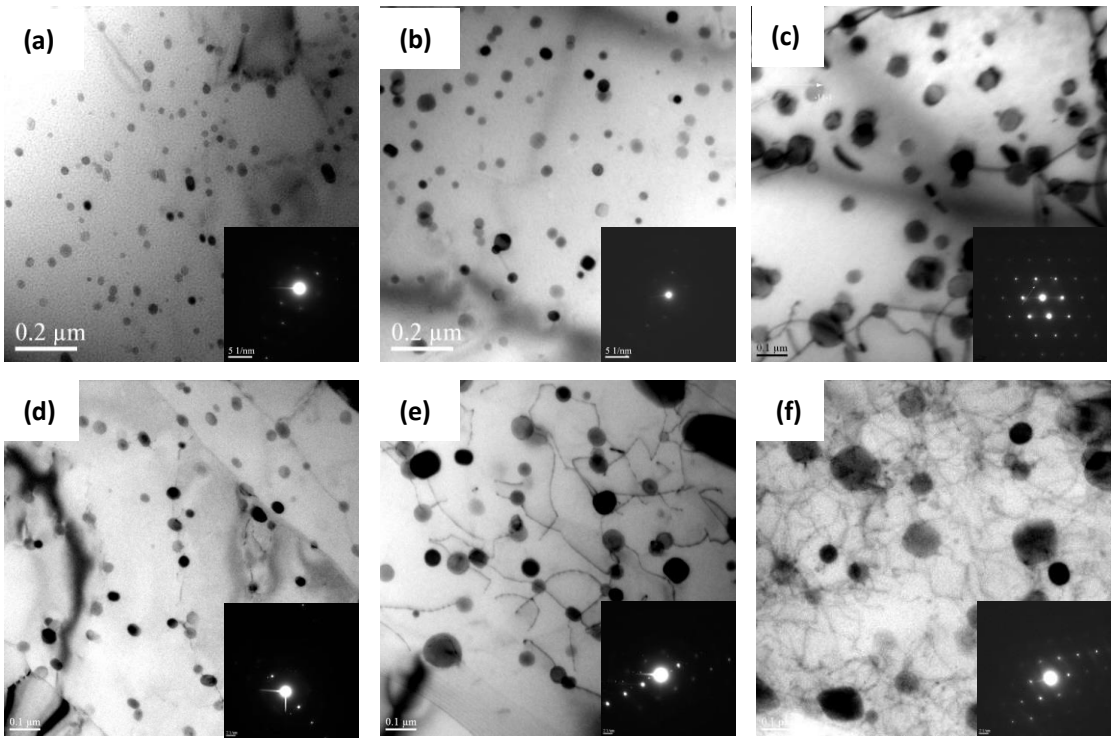

Fig. 4.11 TEM images of Alloy B (a, b, c) and Alloy C (d, e, f) in as-roll condition and annealing at 500 ℃ for 1 and 8 hours respectively.

Table 4.1 Volume fraction and equivalent diameter of dispersoids in of the experimental alloys

Alloy	Terms	As-roll	500℃/1h	500℃/8h
B	Volume fraction	1.8%	1.9%	3.3%
	Diameter	36.5 nm	44.0 nm	86.3 nm
C	Volume fraction	2.7%	3.3%	3.6%
	Diameter	46.8 nm	83.6 nm	95.5 nm

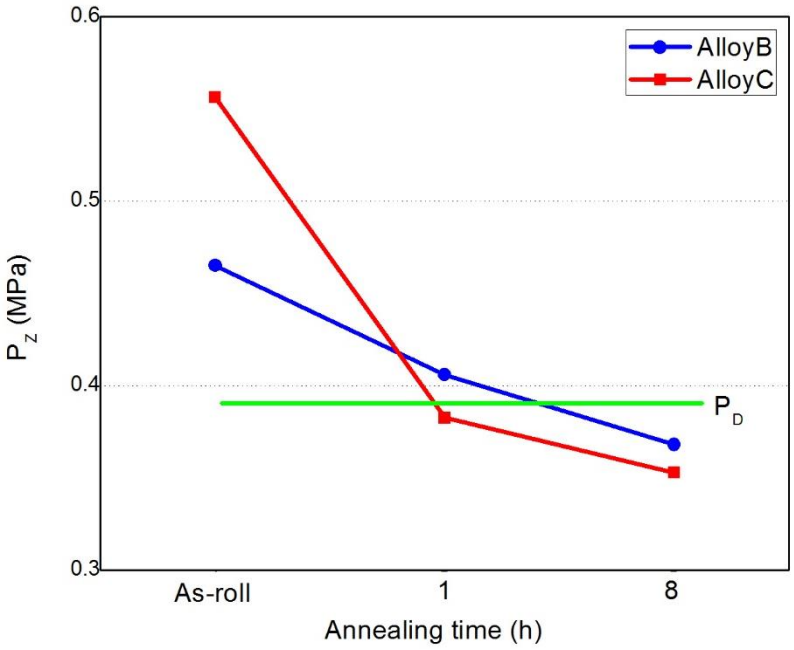

Fig. 4.12 The driving (P_D) and pinning force (P_Z) along with the annealing time of Alloy-B and Alloy-C.

The occurrence of nucleation and growth of recrystallized grains was usually determined by the following equation [12],

$$P = P_D - P_Z = \frac{3\gamma_s}{D} - \frac{3F_V\gamma_s}{d} \tag{4.4}$$

Where P_D is the driving force, P_Z is the pinning force, γ_s is the specific grain boundary energy, D is the diameter of the recrystallized grain, D~2.5 μm for diameter of nuclei

of recrystallized grains and γ_s~0.32 Jm^{-2} were estimated. F_v and d are the volume fraction and equivalent diameter of particles respectively. If $P_D > P_Z$, then the recrystallization will occur and vice versa.

The calculated driving force (P_D) and pinning force (P_Z) with the data in Table 4.1 for the conditions of as-rolled and post-deformation annealing was depicted in Fig. 4.12. As indicated, P_Z of Alloy-C was superior to that of Alloy-B in as-rolled condition and both of them were larger than P_D, suggesting a severe inhibition of recrystallization in as-rolled Alloy-B and Alloy-C, confirming by the low X_v in Alloys-B and C compared with Alloy-A and even lower X_v value in Alloy-C than Alloy-B (Fig. 4.10). However, after 1 hour's annealing at 500 ℃, P_Z of Alloy-C deteriorated rapidly to a value even lower than P_D after while P_Z of Alloy-B dropped less and still larger than P_D. Therefore, the recrystallization in Alloy-C had started but it was still stagnated in Alloy-B, which is also shown in Fig. 4.10 that the X_v is increasing in Alloy-C but it is still low in Alloy-B. When the annealing time extended to 8 hours, P_Z of Alloy-C keeps decreasing due to the coarsening of dispersoids, leading to the further increase X_v in Fig. 4.10. On the other hand, P_Z of Alloy-B also has just decreased below P_D, resulting in a gradually increase of X_v, as shown in Fig. 4.10. Therefore, a faster deterioration in ratio of Fv/d in Alloy-C than Alloy B is the principle reason for the higher X_v though more Mn is added in Alloy C. On the other hand, even after 8 hours' annealing, P_Z of both Alloy-B and Alloy-C were rather close to P_D, which explains the still higher recrystallization resistance in Alloys-B and C than Alloy-A.

As another possible reason, original grain size is reported to affect the recrystallization behavior. Therefore, the average grain size of Alloy-A, Alloy-B and Alloy-C after heat treatment at 400℃/2h were measured based on EBSD mapping images and depicted in Fig. 4.13. It was evident that the grain size decreased with the additions of Mn in the alloys. As shown in Fig. 4.13, the grain size decreases from 421 nm in Alloy-A to 314 nm in Alloy-B and further to 239 nm in Alloy-C. Since the inhomogeneities tended to distribute on grain boundaries, they are favored nucleation sites for recrystallization. Therefore, a higher grain boundary density was expected in Alloy-C with respect to Alloy-A and Alloy-B, which also contributed to the more available nucleation sites in Alloy-C. Therefore, the lower original grain size in Alloy-C can also be a potential reason for its worse recrystallization resistance than Alloy-B. On the other hand, reports [13] also found that coarse grains tend to possess higher strains when subjected to severe deformation, which was one of the important criterion for occurrence of continuous recrystallization [14], which gave the additional information to explain the transition from continuous to discontinuous recrystallization from Alloy-A to Alloy-B and Alloy-C.

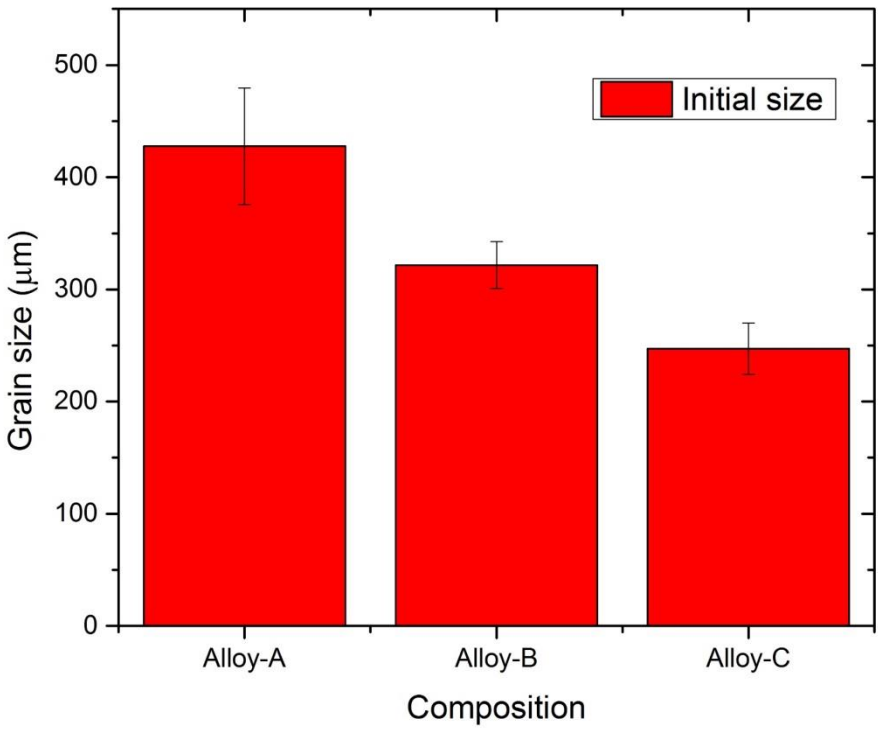

Fig. 4.13 The grain size of alloys after heat treatment at 400℃/2h.

4.3 Summary

In this chapter, precipitation behaviors of Mn-containing dispersoids were systematically studied under different Mn contents and heat treatment parameters. Samples undergoing optimum heat treatment procedure were hot rolled and annealed and their resistance to recrystallization was also quantitatively discussed. The results can be concluded as follows:

1. A Dispersoids precipitated at 350 ℃, reached optimum condition with largest

number density and fine size at 400 ℃ and coarsened above 400 ℃.

2. Mn content had different influence on precipitation behaviors of dispersoids during various heat treatment temperature ranges. At a heat treatment temperature below 400 ℃, a higher Mn content resulted in dispersoids with a higher density but limited size. While at a temperature range higher than 400 ℃, additional Mn content significantly accelerated the coarsening process during soaking, although more dispersoids were still generated.

3. Following hot-rolling and subsequent annealing at 500 ℃, the recrystallization volume fraction is generally increasing with holding time. However, they are much lower in alloy with Mn addition compared with the alloy free of Mn. The addition of Mn also caused transformation of recrystallization behavior from continuous to discontinuous due to the introduction of dispersoids and finer original grain size.

4. Under same post-annealing condition, the recrystallization volume fraction in alloy with 0.5%Mn is lower than that with 1.0%Mn due to the faster deteioration in pinning force from a higher coarsening rate of dispersoids in Alloy-C. Meanwhile, the smaller grain size in alloy with 1.0% Mn also contributed to the faster recrystallization process by inducing more boundary areas which were usually preferred nucleation sites.

REFERENCES

[1] K. Liu, and X.-G. Chen, "Development of Al–Mn–Mg 3004 alloy for applications at elevated temperature via dispersoid strengthening," *Materials & Design*, vol. 84, pp. 340-350, 2015.

[2] L. Lodgaard, and N. Ryum, "Precipitation of dispersoids containing Mn and/or Cr in Al–Mg–Si alloys," *Materials Science and Engineering: A*, vol. 283, pp. 144-152, 2000.

[3] H. WENZL, "ALTENPOHL, D-ALUMINIUM UND ALUMINIUMLEGIERUNGEN," 1966.

[4] F. J. Humphreys, and M. Hatherly, *Recrystallization and related annealing phenomena*: Elsevier, 2012.

[5] F. Humphreys, "Local lattice rotations at second phase particles in deformed metals," *Acta Metallurgica*, vol. 27, pp. 1801-1814, 1979.

[6] H. Jazaeri, and F. Humphreys, "The transition from discontinuous to continuous recrystallization in some aluminium alloys I-the deformed state," *Acta Materialia*, vol. 52, pp. 3239-3250, 2004.

[7] A. Eivani, H. Ahmed, J. Zhou *et al.*, "Correlation between electrical resistivity, particle dissolution, precipitation of dispersoids, and recrystallization behavior of AA7020 aluminum alloy," *Metallurgical and materials Transactions A*, vol. 40, pp. 2435-2446, 2009.

[8] B. Forbord, L. Auran, W. Lefebvre *et al.*, “Rapid precipitation of dispersoids during extrusion of an Al–0.91 wt.% Mn–0.13 wt.% Zr–0.17 wt.% Sc-alloy,” *Materials Science and Engineering: A,* vol. 424, pp. 174-180, 2006.

[9] I. Nikulin, A. Kipelova, S. Malopheyev *et al.*, “Effect of second phase particles on grain refinement during equal-channel angular pressing of an Al–Mg–Mn alloy,” *Acta materialia,* vol. 60, pp. 487-497, 2012.

[10] M. Somerday, and F. Humphreys, “Recrystallisation behaviour of supersaturated Al–Mn alloys Part 1–Al–1.3 wt-% Mn,” *Materials science and technology,* vol. 19, pp. 20-29, 2003.

[11] S. Tangen, H. Bjerkaas, T. Furu *et al.,* "The Effects of Dispersoids on the Recrystallization Behavior in a Cold Rolled AA 3103-Aluminium Alloy." *Materials Forum,* vol. 28, pp. 1229-1234, 2004.

[12] L. E. Murr, “Interfacial phenomena in metals and alloys,” *Addison-Westly Publ,* pp. 387, 1975.

[13] L. Ryde, W. Hutchinson, and S. Jansson, “Recrystallization mechanisms, kinetics and textures in cold rolled copper,” *Recrystallization,* vol. 90, pp. 313-318, 1990.

[14] H. Jazaeri, and F. Humphreys, “The transition from discontinuous to continuous recrystallization in some aluminium alloys: II–annealing behaviour,” *Acta Materialia,* vol. 52, pp. 3251-3262, 2004.

CHAPTER 5

EFFECT OF SC, ZR ADDITIONS ON MN-CONTAINING DISPERSOIDS AND PROPERTIES

This chapter aims at clarifying the influence of Zr and Sc additions on Mn-containing dispersoids in Al-Mg-Si 6082 alloys. For this purpose, 6082 alloys containing only Mn and alloys with additional Zr (and Sc) were subjected to different heat treatment temperatures and compared. Special emphasis was placed on the complementary precipitation behaviors of dispersoids from different families, including number density, equivalent diameter and volume fraction as a function of heat treatment temperatures and time, which was designed ranging from the precipitation stage to the coarsening stage of each dispersoids family. Finally, the influence of addition of Sc and Zr on the recrystallization resistance after rolling was preliminary investigated.

5.1 Evolution of electrical conductivity

In order to evaluate the concentration of different solutes in the solid solution, electrical conductivity (EC) of Alloy-C, Alloy-D and Alloy-E subjected to the given heat treatment conditions ranging from 350-500 ℃ for up to 24 hours was measured and depicted in the form of 1/EC as a function of heat treatment temperatures and

holding times, as shown in Fig. 5.1. As indicated in equation (5.1), 1/EC was proportional to and mainly influenced by concentration of Mn, Fe, Zr and Sc solutes, while the effect of Si and Mg solutes could be neglected due to the relatively small coefficients [1, 2].

$$1/EC = 0.0267 + 0.032\,Fe_{ss}\% + \mathbf{0.033Mn_{ss}\%} + \mathbf{0.0195Zr_{ss}\%} + \mathbf{0.0192Sc_{ss}\%} + 0.0068Si_{ss}\% + 0.003Mg_{ss}\% \quad (5.1)$$

Additionally, most of Fe solutes was reported to precipitate in the form of intermetallics during casting, thus Fig. 5.1 was a reflection of Mn, Zr and Sc solutes remained in the solid solution after the experimental heat treatments. All of the 1/EC curves in Figs. 5.1 a-c exhibited an initial drop at the beginning of heat treatment and gradually approached a plateau with increasing the temperature or extending the soaking time. It can be seen that, until 450 ℃, all of the three curves reached steady state before 8 hours' holding. However, the plateaus of Alloy-D and E were of higher values than that of Alloy-C, indicating higher solid solution levels remained in Alloy-D and E at steady state.

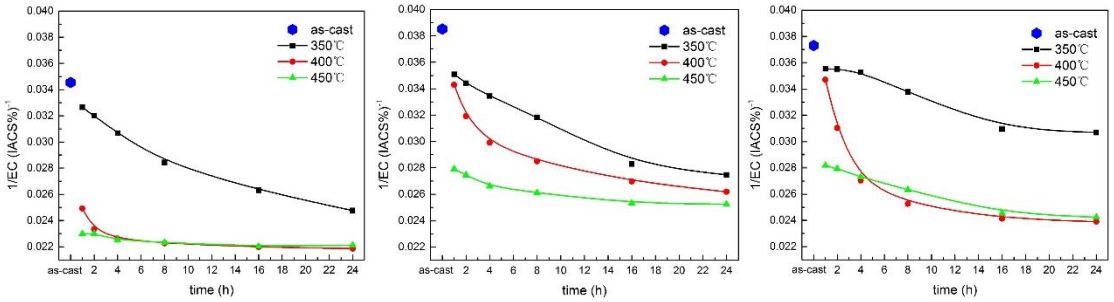

(a) (b) (c)

Fig. 5.1 1/EC curves of (a) Alloy-C, (b) Alloy-D and (c) Alloy-E as a function of heat treatment temperatures and time.

A comparison of 1/EC values at as-cast and steady state (450℃/24h) of all the three alloys was listed in Tab. 5.1. As demonstrated, 1/EC is a reflection of solid solution content of Mn, Zr, Sc solutes in the present study, thus $\Delta 1/EC_{D\text{-}C}$ and $\Delta 1/EC_{E\text{-}C}$ at as-cast condition were resulted from additional Zr and both Zr and Sc solid solutes in Alloy-D and E respectively. In addition, $\Delta 1/EC_{D\text{-}C}$ and $\Delta 1/EC_{E\text{-}C}$ at as-cast condition were of similar values with those at steady state, therefore, the contribution of Zr and Sc in the solid solution to 1/EC in Alloy-D and E can be treated as constant under given heat treatment conditions.

Table 5.1 1/EC values $(\%IACS)^{-1}$ of Alloy-C, D and E and their difference at as-cast state and after heat treatment at 450 ℃ for 24 hours

	$1/EC_{Alloy\text{-}C}$	$1/EC_{Alloy\text{-}D}$	$1/EC_{Alloy\text{-}E}$	$\Delta 1/EC_{D\text{-}C}$	$\Delta 1/EC_{E\text{-}C}$
As-cast	0.0346	0.0385	0.0373	0.0039	0.0027
Heat treated	0.0221	0.0252	0.0242	0.0031	0.0021

5.2 Precipitation behaviors and interaction between dispersoids

After removal of contribution of Zr and Sc solutes to 1/EC values of Alloy-D and E, comparison of modified 1/EC curves reflecting only Mn solid solution levels of Alloy-C, D and E at lower temperature ranges (<450 ℃) was shown in Fig. 5.2, which revealed a rather interesting phenomena.

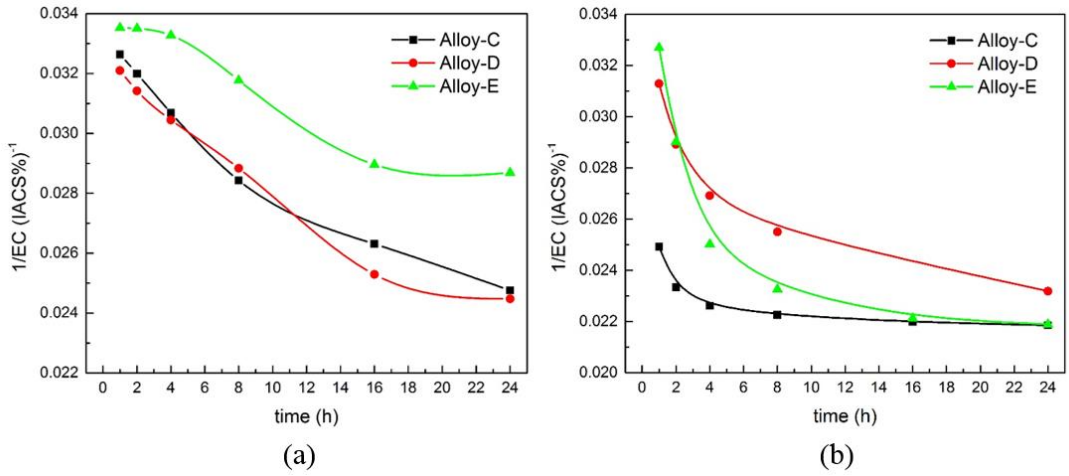

Fig. 5.2 Comparison of 1/EC curves of Alloy-C, Alloy-D and Alloy-E after removal of contribution of equilibrium Zr solutes after heat treatment at (a) 350 ℃ and (b) 400 ℃.

At 350 ℃, as shown in Fig. 5.2a, all of the three curves decreased with the soaking time, but unlike curves of Alloy-C and D which interwined with each other, that of Alloy-E was separated from them, decreasing at an apparently lower speed. That means, at 350 ℃, precipitation of Mn dispersoids was significantly suppressed in Alloy-E which contained both additional Sc and Zr but was not affected in the case of

Alloy-D which only consisted of Zr on the basis of Mn addition. While at 400 ℃, 1/EC curves of both Alloy-D and E initially possessed higher values than that of Alloy-C, however, with extending the soaking time, the curve of Alloy-E approached to and finally overlapped with that of Alloy-C, in contrast of which, that of Alloy-D was still separated from and higher than that of Alloy-C even up to 24 hours. In other words, unlike heat treated at 350 ℃, decomposition of Mn-dispersoids was suppressed throughout the holding at 400 ℃ in the case of Alloy-D, while in the case of Alloy-E, though initially delayed, the decomposition of Mn solutes recovered to the same level as Alloy-C before 24 hours' exposure.

The SEM observation on Mn-dispersoids generated from lower heat treatment temperatures accorded with the previous inference and revealed more details. After heat treatment at 350 ℃ for 24 hours, dispersoids in Alloy-C and D (Figs. 5.3a and b) showed similar amount and size, in great contrast of which, dispersoids in Alloy-E (Fig. 5.3c) were much fewer and slightly bigger. As characterized in Tab. 5.2, both number density and volume fraction of Mn dispersoids in Alloy-E were way smaller than those in Alloy-C and Alloy-D.

After 1 hour's holding at 400 ℃, unlike Alloy-C (Fig. 5.3d) whose Mn-containing dispersoids had already densely distributed, precipitation of Mn-dispersoids in Alloy-D and E (Figs. 5.3e and f) were severely inhibited, exhibiting the much smaller number density and volume fraction, 1.6 μm^{-2} and 1.83% for Alloy-D, 1.0 μm^{-2} and

1.00% for Alloy-E, compared with 11.2 μm^{-2} and 3.14% for Alloy-C. But when heat treatment extended to 24 hours at 400 ℃, Mn-containing dispersoids in Alloy-D evolved into sparsely distributed rod shaped particles (Fig. 5.3h). In great contrast, densely distributed and fine Mn dispersoids were observed in both Alloy-C and E (Fig. 5.3g and i), although the latter were still slightly fewer and larger than the former. Based on the quantitative statistics in Tab. 5.2, it was confirmed that, volume fraction of Mn dispersoids in Alloy-E was similar with that in Alloy-C after 24 hours' exposure at 400 ℃, indicating the decomposition of Mn solutes was no longer suppressed, while the volume fraction of Mn dispersoids in Alloy-D was still smaller than that in Alloy-C, meaning the Mn precipitation was still prohibited at some extent. In summary, the addition of Zr (and Sc) has rather crucial influence on precipitation behavior of Mn dispersoids at heat treatment temperatures under 400 ℃. Additionally, this effect was found even to be varied at 350 and 400 ℃.

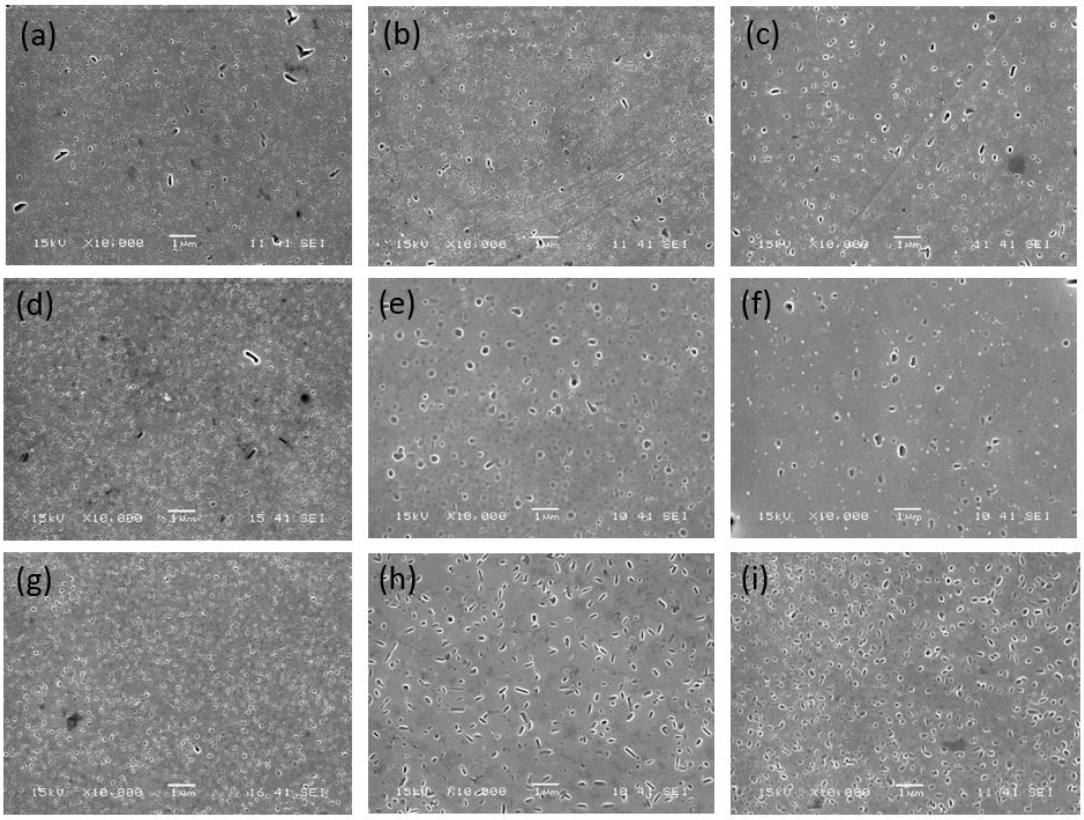

Fig. 5.3 Mn dispersoids in (a) (d) (g) Alloy-C, (b) (e) (h) Alloy-D and (c) (f) (i) Alloy-E after heat treatment at 350 ℃ for 24 hous and 400 ℃ for 1 hour and 24 hours respectively.

Table 5.2 Surface number density (ρ) and area fraction (f) of Mn-containing dispersoids in Alloy-C, D and E at the given heat treatment conditions

		Alloy-C	Alloy-D	Alloy-E
350℃/24h	$\rho/\mu m^{-2}$	15.7	15.1	3.4
	f	3.95%	3.94%	2.01%
400℃/1h	$\rho/\mu m^{-2}$	11.2	1.6	1.0
	f	3.14%	1.83%	1.00%
400℃/24h	$\rho/\mu m^{-2}$	15.8	3.4	8.2
	f	4.62%	4.08%	4.51%

Dark field TEM images taken from the $<001>_{Al}$ diffraction pattern were shown in Fig. 5.4 to reveal the corresponding precipitation behaviors of Al_3Zr and $Al_3(Sc,Zr)$ dispersoids. Huge contrast was displayed between morphologies of Alloy-E after heat treatment at 350 ℃ for 1 and 24 hours, in the former, as shown in Fig. 5.4a were there some amount of relatively big square particles whose <001> plane was parallel with $<001>_{Al}$ but no $Al_3(Sc,Zr)$ dispersoids big enough to be observed in the given magnification, while in the latter, large quantities of $Al_3(Sc,Zr)$ dispersoids exhibited homogenously in the matrix with only very a few square particles left. As indicated by the arrows in Fig. 5.4a, most of the square particles have very strict orientation relationship with the matrix, each length of which was parallel with $<001>_{Al}$, and were also lined up along $<001>_{Al}$. EDS analysis further revealed that, the composition of the square particles were Al(FeMn)Si, which were probably the early stage of Mn-containing dispersoids due to their composition, shape and orientation relationship with Al matrix [3]. On the other hand, similar square particles were also found in Alloy-D after 24 hours' holding at 350 ℃ (Fig. 5.4d) but no presence of Al_3Zr dispersoids was observed.

As heat treatment temperatures raised to 400 ℃, small amount of Al_3Zr dispersoids started to show up in Alloy-D after 24 hours' holding (Fig. 5.4e) and they separated along $<001>_{Al}$, while coarsening of $Al_3(Sc,Zr)$ dispersoids had already occurred in Alloy-E (Fig. 5.4c), compared with the one heat treated at 350 ℃ for 24 hours (Fig.

5.4b), the number density remained nearly identical but the size apparently coarsened. Therefore, the precipitation of Mn-containing dispersoids varied simultaneously with that of Zr, Sc-induced dispersoids. At 350 ℃ where Al_3(Sc,Zr) dispersoids started to precipitate, formation of Mn-dispersoids in alloy containing both additional Sc and Zr were suppressed, while at 400 ℃ where nucleation of Al_3Zr dispersoids occurred, and Al_3(Sc,Zr) dispersoids coarsened, precipitation of Mn-dispersoids was inhibited in Alloy-D while no longer delayed in Alloy-E.

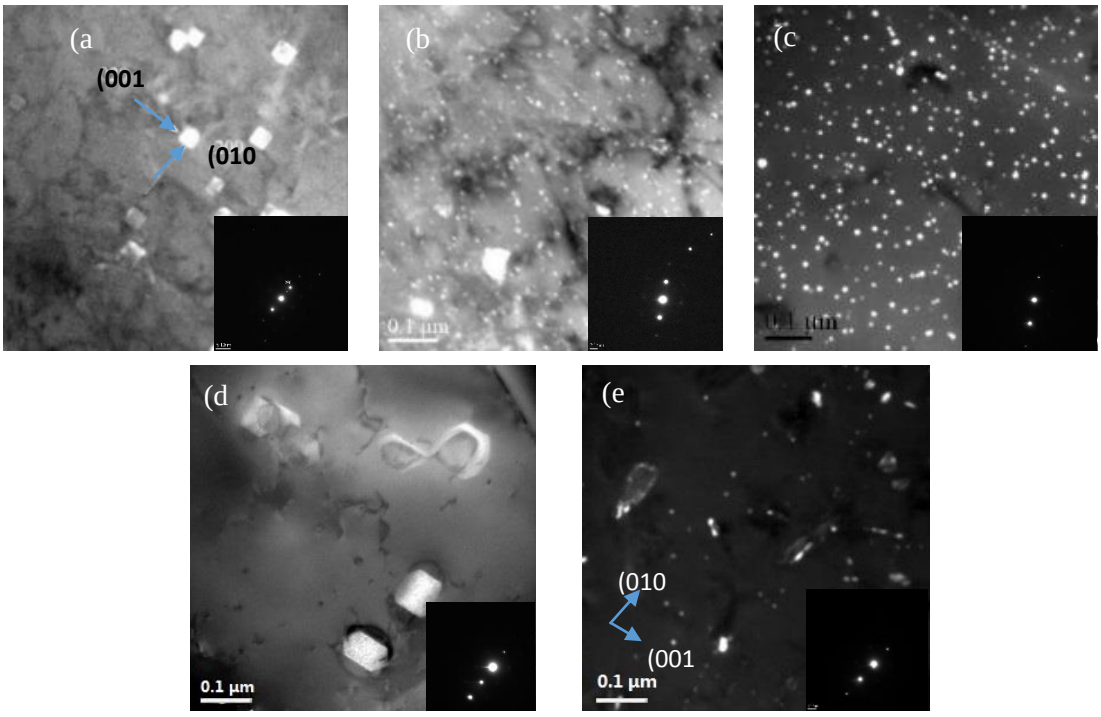

Fig. 5.4 Dark field TEM images of (a) – (c) Alloy-E after heat treatment at 350 ℃ for 1 and 24 hours, 400 ℃ for 24 hours respectively and Alloy-D after heat treatment at (d) 350 ℃ for 24 hours and (e) 400 ℃ for 24 hours.

While at higher temperature ranges (>450 ℃), the difference between modified 1/EC curves of Alloy-C, D and E was no longer as obvious after removal of Sc, Zr contribution, as shown in Fig. 5.5, they all decreased slightly with extending the soaking time and eventually became identical at 24 hours.

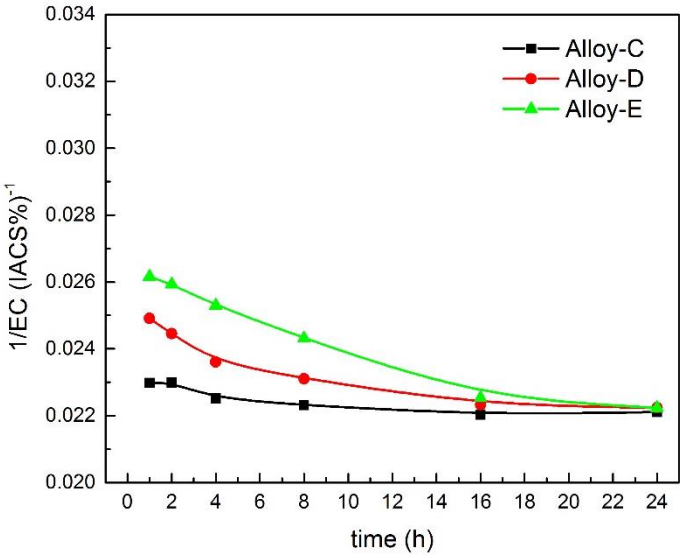

Fig. 5.5 Comparison of 1/EC curves of Alloy-C, Alloy-D and Alloy-E after removal of contribution of equilibrium Zr solutes after heat treatment at 450 ℃.

By comparing SEM images of Mn-dispersoids of Alloy-C, D and E taken after 1 hour's (Fig.6 a-c) to those after 24 hours' (Fig. 5.6 d-f) exposure at 450 ℃, it was apparent that regardless of different composition of the three alloys, their dispersoids all went through the coarsening process, in other words, some of the particles coarsened at the expense of dissolution of small ones. It was also noteworthy that, under the same heat treatment parameters, dispersoids in Alloy-D and Alloy-E always

exhibited in larger size but fewer density than the ones in Alloy-C (comparing among Figs.2 a-c or d-f), which indicated that, the addition of Zr (and Sc) accelerated the coarsening process of Mn-dispersoids at higher temperature ranges. The observation was in agreement with the quantitative analysis shown in Figs. 5.6g and h, which quantified the surface number density and circular diameter in details. In general, the number density of all the three alloys decreased rapidly with the holding time. However, the density of dispersoids in Alloy-C had a higher initial value around 10.4 μm^{-2} and its reduction speed was sharp until reaching around 8.6 μm^{-2} at 8 hours but slowed down afterwards, maintaining an almost steady density around 8.1 μm^{-2} at 24 hours. While density of dispersoids in Alloy-D and E started with lower values and reduced more quickly than that in Alloy-C until hitting around 4.7 μm^{-2} at 24 hours. Meanwhile, the circular diameter of dispersoids in all the three alloys increased with time extending. Similar with the trend of density, the diameter in Alloy-C rapidly increased from 83.65 nm at 1 hour to 93.15 nm at 8 hours and slowed down significantly afterwards, which was merely 95.81 nm at 24 hours. On the other hand, the size in Alloy-D and E coarsened much quicker than the case of Alloy-C, from 92.5 and 96.88 nm at 1 hour to 124.81 and 122.52 nm at 24 hours. Though the coarsening process was obviously accelerated with addition of Zr (and Sc) at 450 ℃, the overall area fraction of dispersoids was not significantly affected in Alloy-D or E, as indicated in Fig. 5.6i, all the curves of area fraction which belonged to three different alloys stabilized and wrapped together after 2 hours' exposure. In other

words, the remained Mn solutes in the solid solution were of similar amount in Alloy-C, D and E.

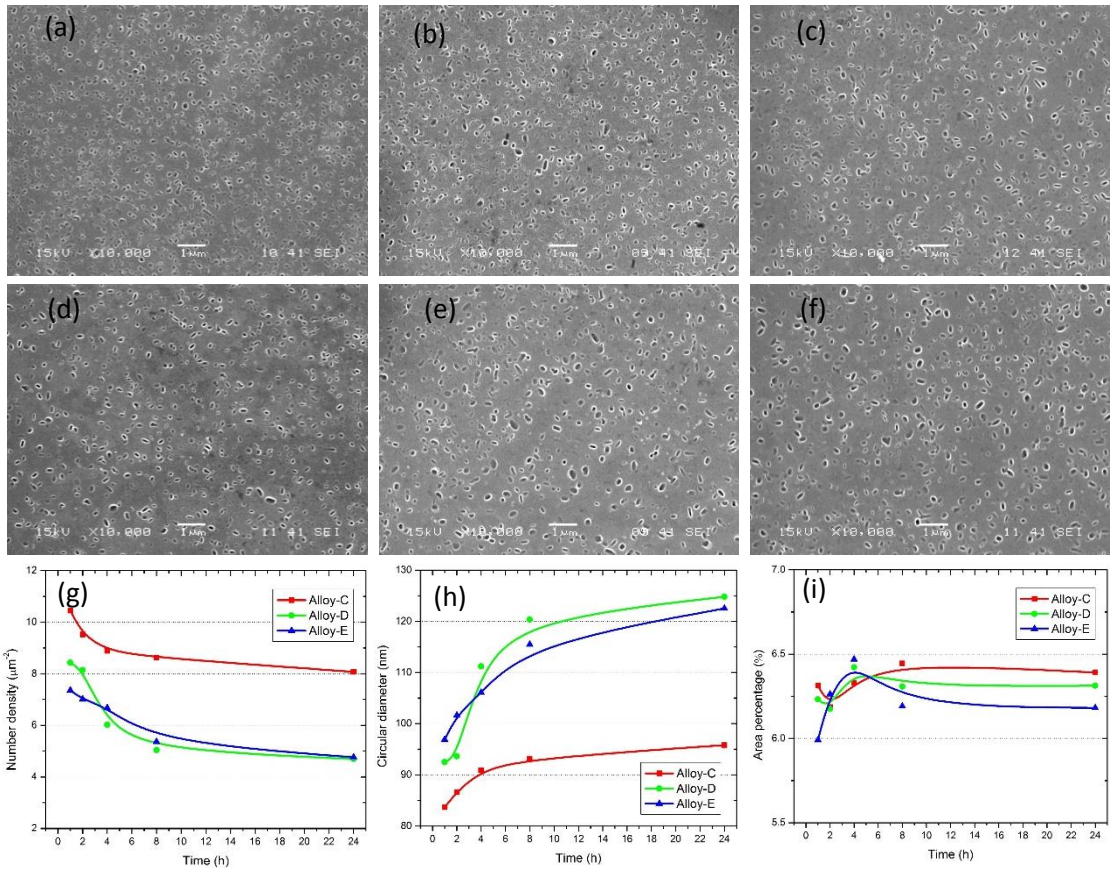

Fig. 5.6 Mn dispersoids in (a) and (d) Alloy-C, (b) and (e) Alloy-D, (c) and (f) Alloy-E after heat treatment at 450 ℃ for 1 and 24 hours respectively and their (g) surface number density, (h) circular diameter and (i) area fraction.

To reveal the corresponding formation of Al_3Zr or $Al_3(Sc,Zr)$ disersoids in Alloy-D and E at higher temperature ranges, dark field TEM images were taken, as shown in Fig. 5.7. As indicated in Fig. 5.7a, $Al_3(Sc,Zr)$ dispersoids in Alloy-E coarsened additionally compared with those after heat treatment at 400 ℃ for 24 hours (Fig.

5.4c). On the other hand, Al_3Zr dispersoids in Alloy-D also possessed a bigger size (Fig. 5.7b) compared with those obtained at 400 ℃ (Fig. 5.4e) but appeared in the form of clusters. In addition to that, most sets of clusters made up into a perfect square and the length of the square was parallel with $<001>_{Al}$, which coincidently to be in the shape of the square particles shown in Fig. 5.4d. If regarding each set of clusters as a unit, most of these units also distributed along the (001) plane of the Al matrix.

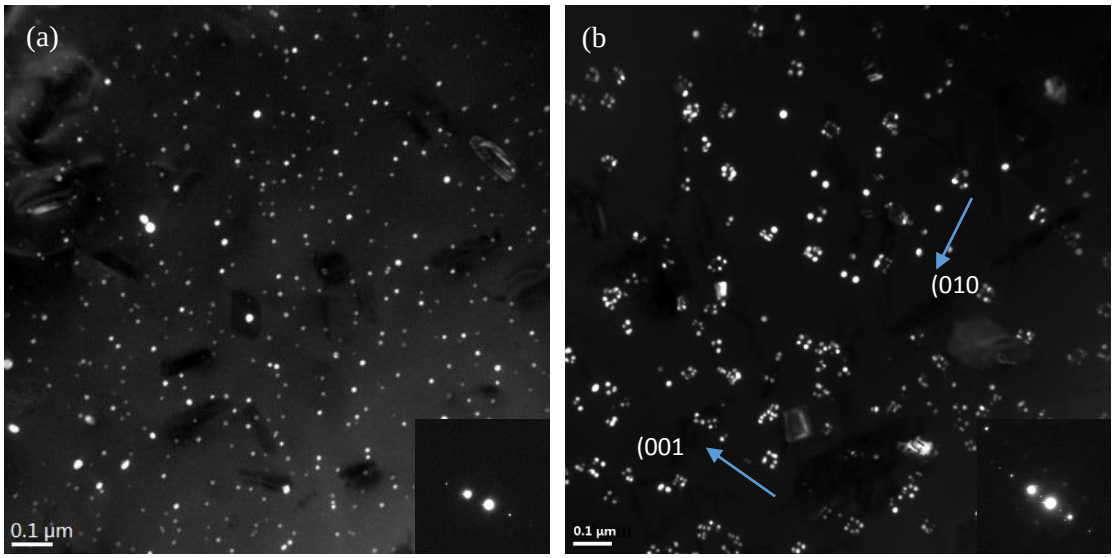

Fig. 5.7 Dark field TEM images of (a) Alloy-E and (b) Alloy-D after heat treatment at 450 ℃ for 24 hours.

5.3 Combined effect of dispersoids on properties

The combined strengthening effect of dispersoids from different families were characterized through vikers-hardness test and as expected, showed various influence under different heat treatments. For instance, after heat treatment at 400 ℃ (Fig. 5.8a),

Alloy-E, with combined additional Sc and Zr additions, possessed far superior micro-hardness than Alloy-C, since $Al_3(Sc,Zr)$ dispersoids precipitated in large quantities and precipitation of α-Al(Fe,Mn)Si dispersoids were no longer suppressed at the given temperature. While Zr in Alloy-D played a negligible and sometimes even detrimental role on micro-hardness at 400 ℃ compared with Alloy-C, since formation of Mn-containing dispersoids was significantly inhibited, leading to a loss of dispersive strengthening, which competed with the hardening effect induced by small amount of Al_3Zr dispersoids and remained Zr solutes in the solid solution. At 450 ℃ (Fig. 5.8b), however, both Alloy-D and Alloy-E exhibited higher hardness than Alloy-C, since precipitation of Mn-containing dispersoids were not resisted in neither cases. Although a loss in strength was caused by fewer and coarser Mn dispersoids in Alloy-D and E, compared with strength effect induced by large amount of Al_3Zr and $Al_3(Sc,Zr)$ decompositions, this loss can be neglected.

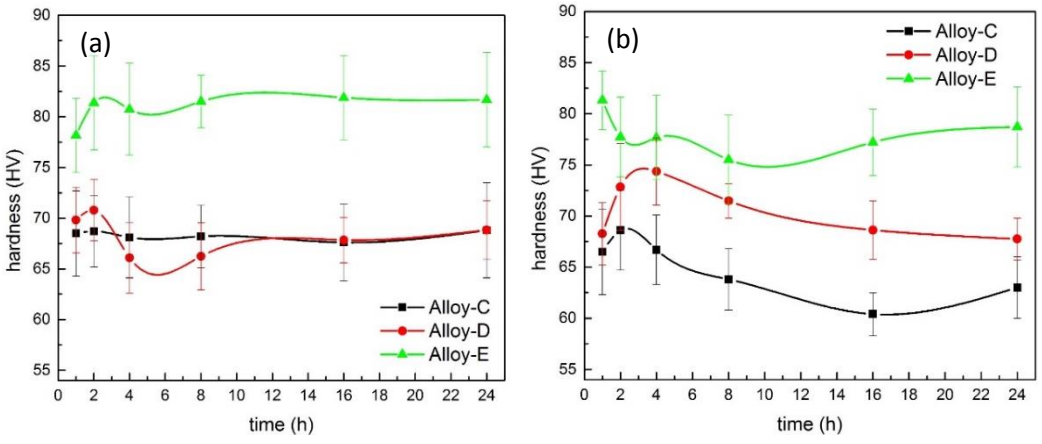

Fig. 5.8 Comparison of Vikers-hardness of Alloy-C, D and E after heat treatment at (a) 400 ℃ and (b) 450 ℃.

After heat treatment at 400℃, Alloy-C, Alloy-D and Alloy-E were subjected to hot rolling at 400℃ and subsequent annealing at 500℃ for up to 8 hours in order to identify their resistance to recrystallization. Orientation maps were shown in Fig. 5.9. Following the hot-rolling, elongated bands dominated microstructures of all the three alloys, between boundaries of which were there distribution of recrystallized fine grains. The quantities of recrystallized grains in as-rolled Alloy-D, however, were obviously more than those of Alloy-C and Alloy-E. After 1 hour's annealing, deformed bands still dominated the main structures in Alloy-E, while in Alloy-C and Alloy-D, more sites became available for recrystallization, the elongated grians started to be consumed and separated by the recrystallizing grains. As annealing time extended to 8 hours, although in a smaller proportion, elongated bands could still be observed in Alloy-C and Alloy-E, but a large extent of recrystallization had already occurred in Alloy-D, barely no deformed bands can be observed, instead of which, low angle boundary free recrystallizing grains made up a great fraction.

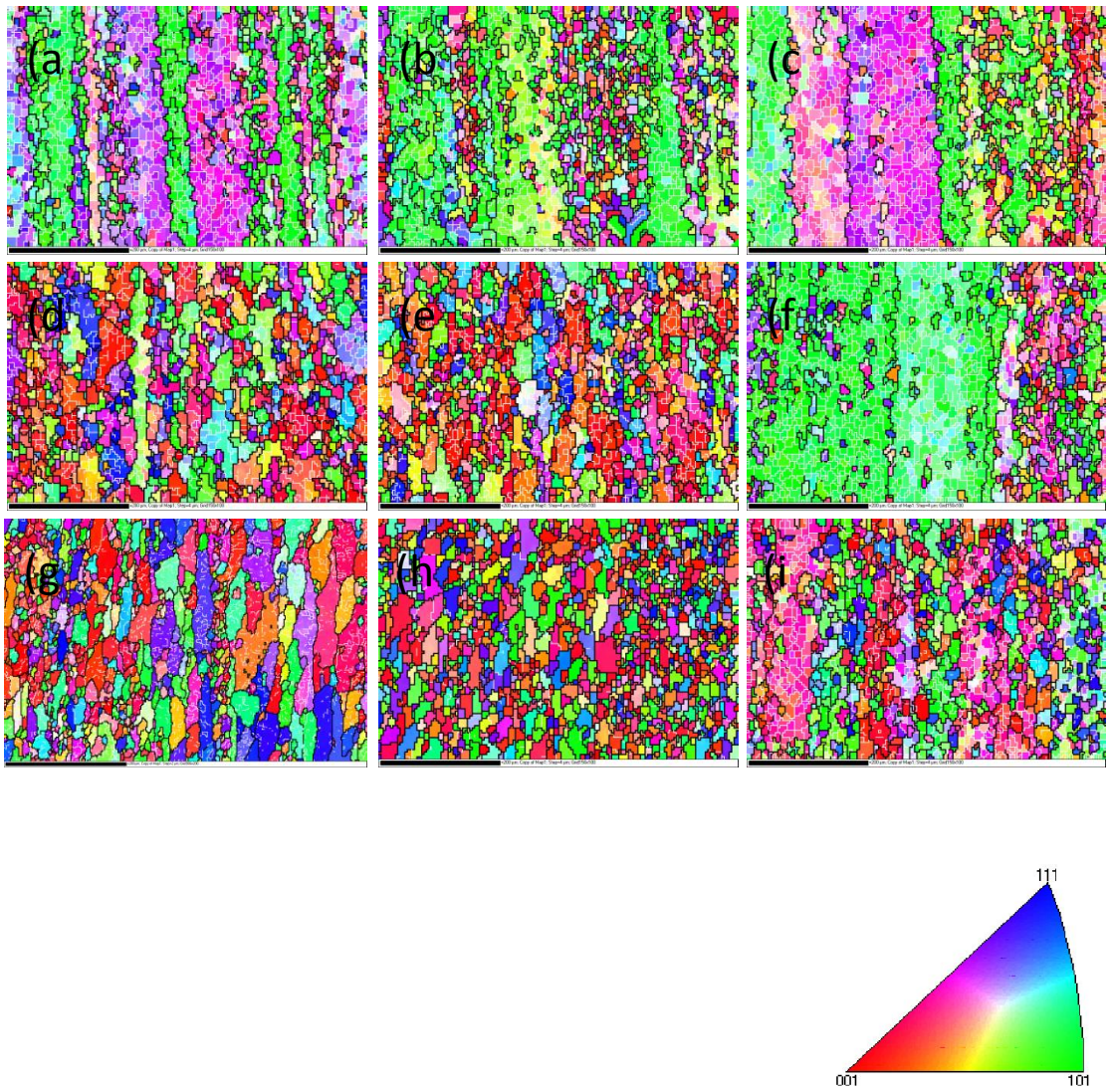

Fig. 5.9 Orientation maps of Alloy C (a, d, g), Alloy D (b, e, h) and Alloy E (c, f, i) following hot rolling and subsequent annealing at 500 ℃ for 1 and 8 hours respectively.

The observation was in line with the measured recrystallization volume fraction as a function of the annealing time, as shown in Fig. 5.10. Generally, compared with alloy with only Mn addition, simultaneous addition of Mn and Zr hugely accelerated the recrystallization process, until 8 hours' annealing, the proportion of recrystallization

increased from 52.3% for Alloy-C to 75.6% for Alloy-D. On the contrary, simultaneous addition of Mn, Zr and Sc led to an enhancement in the recrystallization resistance, the proportion of recrystallization in Alloy-E was still lower than 30% even annealing at 500℃ for 8 hours. This controversial resistance effect on recrystallization resulted from Zr and both Sc, Zr additions can also be attributed to varied precipitation behaviors of different types of dispersoids under preheat treatment at 400 ℃.

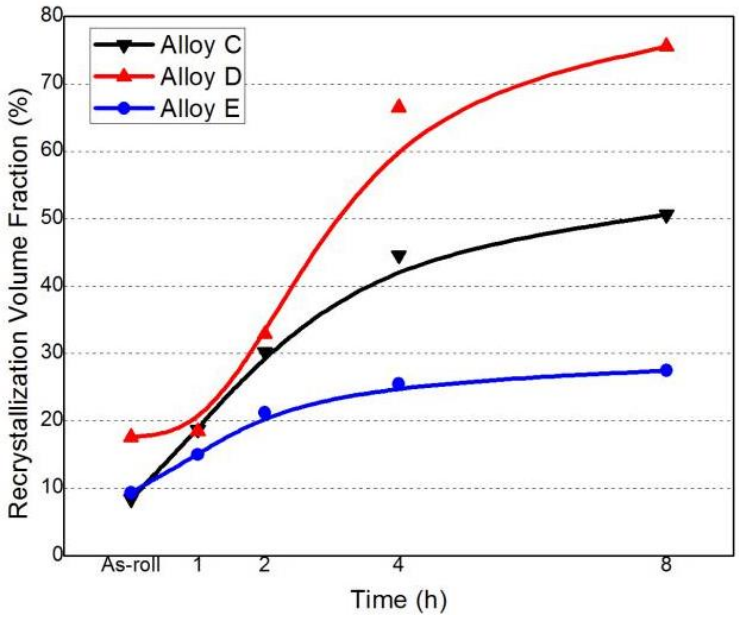

Fig. 5.10 Recrystallization volume fraction of alloys following hot-rolling and subsequent annealing

5.4 Discussion

Two factors could be responsible for the influence of Sc, Zr additions on the precipitation behaviors of Mn-containing dispersoids, namely the inducement of additional Zr (and Sc) solutes in the solid solution and the formation of Al_3Zr and $Al_3(Sc,Zr)$ dispersoids. The first explanation can be excluded due to the following reasons. First of all, as observed in the following section, there was always certain amount of Zr (and Sc) solutes remained in the solid solution throughout all temperature ranges. However, in great contrast with this consistency of Zr (and Sc) solid solutes, precipitation of Mn dispersoids was not always inhibited under different temperatures. Some may argue that segregation of Zr solutes on dislocations and interface between other particles and matrix could prevent the diffusion of Mn solutes, thus inhibiting the precipitation of Mn dispersoids. But if such segregation mattered, the precipitation of Mn dispersoids should be suppressed at 350 ℃ in the case of Alloy-D which was apparently contradicted with the fact that the volume fraction of Mn dispersoids in Alloy-D was similar with that in Alloy-C after 24 hours' holding at 350 ℃. Contrarily, the second explanation matched very well with the experimental results. Under heat treatment at 350 ℃, where precipitation of Al_3Zr dispersoids in Alloy-D had not yet started even at 24 hours, decomposition of Mn dispersoids was not resisted. While in Alloy-E where $Al_3(Sc,Zr)$ dispersoids were dominated by precipitation, Mn dispersoids were significantly suppressed. Additionally at 400 ℃, where a few Al_3Zr dispersoids were observed in Alloy-D after 24 hours' holding,

indicating which was the precipitation temperature of Al_3Zr dispersoids, Mn decomposition was prohibited. While in Alloy-E where most of $Al_3(Sc,Zr)$ dispersoids had already coarsened at 24 hours, Mn decomposition was only initially suppressed and recovered to the extent as Alloy-C before 24 hours. As temperature raised above 450 ℃, where coarsening occurred in both Alloy-D and Alloy-E, sign of suppression on Mn dispersoids was no longer found. In a word, it was the precipitation behavior of Zr (and Sc) dispersoids that inhibited decomposition of Mn dispersoids.

Microstructures of Alloy-D provided some indications on mechanism of interactions between Al_3Zr dispersoids and Mn dispersoids, which was Al_3Zr dispersoids preferred to nucleate on u-phases, and thus inhibited the formation of Mn-containing dispersoids which regarded u-phases as preferential nucleation sites. As shown in Fig. 5.11a, rod-shaped particles were observed distributed along $<001>_{Al}$ in Alloy-D after heat treatment at 400 ℃ for 1 hour through dark field image taken from $[001]_{Al}$ direction at 2 beam condition. Their orientation relationship with Al matrix, morphology and compositions (Fig. 5.11b) indicated that, these particles were u-phases [3], whose $<001>_u$ was parallel with $<010>_{Al}$. It was noteworthy that small amount of Zr was also detected in the u-phase. As time extended to 24 hours, most of u-phases disappeared, while Al_3Zr dispersoids precipitated linearly along $<001>_{Al}$, the same orientation with u-phase, which indicated that, Al_3Zr dispersoids nucleated on u-phases and consumed the latter. And even though coarsened and exhibited in the

form of rectangular clusters at 450℃/24h (Fig. 5.11d), they each group of clusters still lined up on $<001>_{Al}$. What's more, these square clusters of Al_3Zr dispersoids possessed the shape and orientation relationship with Al matrix which were coincidently identical with those of early stage of Mn-containing dispersoids (Fig. 5.4d) which were also known to nucleate on u-phases [3]. This was because the former rod shaped u-phases tended to break into small equiaxed particles and transformed gradually into α-Al(Fe,Mn)Si dispersoids, and this process was accelerated by a higher temperature. Therefore, Al_3Zr dispersoids nucleated on these u-phases exhibited in the form of rectangular clusters at higher temperatures. Such coincidently similar shape of Al_3Zr clusters with other phases were also respectively observed in alloys containing Al_2Cu and η'-phase, and have been attributed to the preferential nucleation on these phases by researchers [4, 5]. TEM bright field images of Alloy-D were shown in Fig. 5.12 as an evidence of competing precipitation between Al_3Zr and Mn-containing dispersoids on u-phases. Through EDS detection, coarse Mn-containing dispersoid was observed to be attached with the u-phase which did not contain Zr (Fig. 5.12a). While for the u-phase which was detected to include Zr, no Mn-containing dispersoids were observed attached to it (Fig. 5.12b)

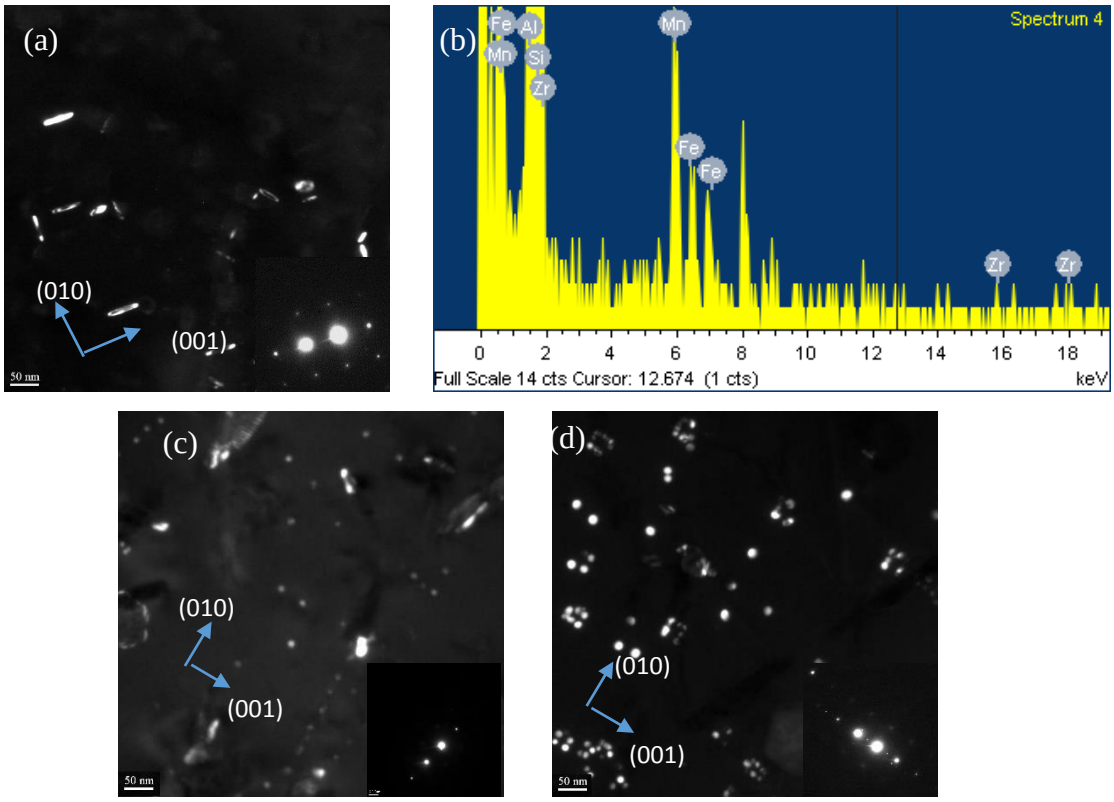

Fig. 5.11 Dark field images of Alloy-D after heat treatment at 400 ℃ for (a) 1 hour and (b) EDS results of its rod-shaped particles, (c) for 24 hours and (d) at 450 ℃ for 24 hours.

Therefore it was reasonable to infer that Al_3Zr dispersoids nucleated on u-phase, leading to dissolution of the latter when it came to the precipitation temperature of Al_3Zr thus preventing the formation of α-dispersoids. As a result, fewer and coarser dispersoids were always observed in Alloy-D even the decomposition of Mn dispersoids were no longer inhibited at higher temperature ranges, since fewer sites were left to be available for the formation of Mn dispersoids after the consumption of u-phases.

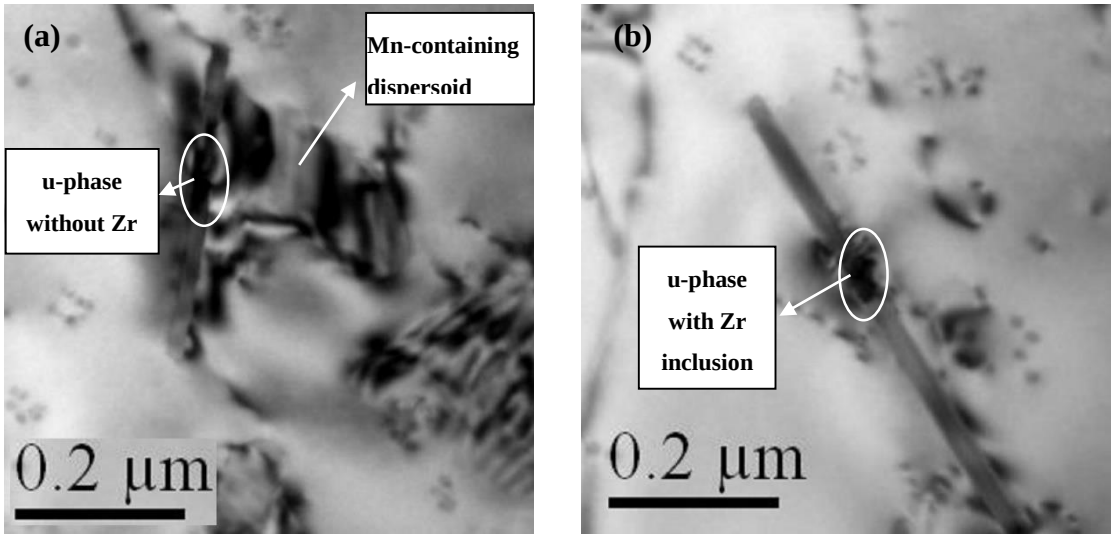

Fig. 5.12 TEM bright field images showing (a) u-phase without Zr inclusion and (b) u-phase containing Zr taken from Alloy-D after heat treatment at 450 ℃ for 24 hours.

Since nucleation of $Al_3(Sc,Zr)$ dispersoids also led to the suppression of Mn-containing dispersoids, similar mechanism might be applied. However, neither linearly distribution nor clusters of $Al_3(Sc,Zr)$ dispersoids were observed in the present study, which probably because they can also precipitate homogenously on many other sites in large quantities, application of such mechanism to alloys containing both additional Sc and Zr remained skeptical.

5.5 Summary

The different influence of Zr (and Sc) additions on Mn-containing dispersoids in AA6082 alloys had been clarified in the present work under different heat treatment parameters. It was found that interactions between them depended highly on the heat

treatment temperatures. At 350 ℃ where Al_3(ScZr) dispersoids started to precipitate while Al_3Zr had not formed, combined addition of Sc and Zr significantly inhibited precipitation behaviors of Mn dispersoids while solo Zr addition had negligible influence. At 400 ℃ where Al_3Zr just precipitated and Al_3(Sc,Zr) dispersoids started coarsening, Zr addition severely delayed Mn precipitation even holding for up to 24 hours while joint Sc, Zr additions only suppressed Mn decomposition at early stage before 16 hours. On the other hand, at temperatures above 450 ℃, neither Zr nor joint Sc and Zr additions inhibited precipitation of Mn dispersoids, though coarser and fewer Mn dispersoids were obtained. Linerly distributed and blocky clusters of Al_3Zr dispersoids were observed in sequence with increasing the heat treatment temperature. Providing that inclusion of Zr in u-phase were detected in alloys with Zr addition, a theory was proposed that, Al_3Zr dispersoids preferred to nucleate on u-phases and consumed the latter simultaneously, therefore suppressing precipitation of Mn-containing dispersoids. Though not confirmed, there was some indication that such mechanism might also be applied to Al_3(Sc,Zr) dispersoids.

As expected, the hot-rolled alloys with different composition showed controversial recrystallization resistance after pre-heat treatment at 400 ℃ for 2 hours, the alloy with combined Sc, Zr addition showed superior inhibiting effect while the alloy with solo additional Zr weakened the resistance to recrystallization compared with the base Al-Fe-Mn-Si alloy.

REFERENCES

[1] K. Liu, and X.-G. Chen, "Development of Al–Mn–Mg 3004 alloy for applications at elevated temperature via dispersoid strengthening," *Materials & Design*, vol. 84, pp. 340-350, 2015.

[2] R.-z. Chao, X.-h. Guan, R.-g. Guan *et al.*, "Effect of Zr and Sc on mechanical properties and electrical conductivities of Al wires," *Transactions of Nonferrous Metals Society of China*, vol. 24, pp. 3164-3169, 2014.

[3] L. Lodgaard, and N. Ryum, "Precipitation of dispersoids containing Mn and/or Cr in Al–Mg–Si alloys," *Materials Science and Engineering: A*, vol. 283, pp. 144-152, 2000.

[4] D. Tsivoulas, J. D. Robson, C. Sigli *et al.*, "Interactions between zirconium and manganese dispersoid-forming elements on their combined addition in Al–Cu–Li alloys," *Acta Materialia*, vol. 60, pp. 5245-5259, 2012.

[5] J. D. Robson, and P. B. Prangnell, "Dispersoid precipitation and process modelling in zirconium containing commercial aluminium alloys," *Acta Materialia*, vol. 49, pp. 599-613, 2001.

CHAPTER 6

CONCLUSIONS AND FUTURE WORK

6.1 Conclusions

The main conclusions of this thesis can be summarized as followings:

1. In Al-Si-Mg 6082 alloys, the Mn-containing dispersoids showed different precipitation behaviors under various heat treatment temperatures. At a temperature <= 400 ℃, nucleation and growth dominated the precipitation of dispersoids while at higher temperatures, coarsening became the main mechanism.

2. The Mn addition level had different influences on precipitation behavior of dispersoids at various heat treatment temperatures. At low heat treatment temperature <= 400 ℃, the high Mn content resulted in the formation of dispersoids with a high density but small size. While at high temperature >400 ℃, the high Mn significantly accelerated the coarsening process during soaking, although more dispersoids were still generated.

3. Following hot-rolling and subsequent annealing at 500 ℃, the recrystallization

volume fraction is generally increasing with holding time. However, the recrystallization is much lower in the alloys with Mn addition compared with the base alloy free of Mn. The addition of Mn also caused the recrystallization transferring from continuous to discontinuous due to the introduction of dispersoids and finer original grain size.

4. Under same post-annealing condition, the recrystallization volume fraction in the alloy with 0.5% Mn is lower than that with 1.0% Mn due to the faster deterioration in pinning force by the coarsening of dispersoids in the alloy with 1.0% Mn. Meanwhile, the smaller grain size in the alloy with 1.0% Mn also contributed to the faster recrystallization process by inducing more boundary areas, which were usually preferred nucleation sites.

5. The addition Zr (Alloy-D) or the combined addition of Zr and Sc (Alloy-E) had significant influence on Mn-containing dispersoids at low temperature range (<400 ℃). At 350 ℃, when Al_3(Sc,Zr) dispersoids precipitated in large quantities, the formation of Mn-containing dispersoids was severely delayed in Alloy-E but Mn-dispersoids in Alloy-D were less affected because Al_3Zr did not precipitate yet. At 400 ℃, when Al_3Zr began to precipitate, the precipitation of Mn-containing dispersoids was suppressed in Alloy-D.

6. The effect of Zr and Sc addition on Mn-containing dispersoids was less prominent at heat treatment temperatures higher than 450 ℃, but fewer and coarser Mn dispersoids were produced in both Alloy-D and Alloy-E.

7. In Alloy-D, Al_3Zr dispersoids preferred to nucleate on u-phases and consumed the latter, and therefore, it suppressed the precipitation of Mn-containing dispersoids. Such mechanism might also be applied to $Al_3(Sc,Zr)$ dispersoids.

8. During post-annealing after hot rolling, the alloy with 0.2% Zr weakened the recrystallization resistance while the alloy with 0.1% Zr and 0.1% Sc addition showed superior recrystallization inhibition compared with the base Al-Mg-Si 6082 alloy.

6.2 Future work

Though a number of results have been obtained in the present study, there still remained many works to be accomplished:

1. In order to achieve even better recrystallization resistance during annealing, a wider range of Mn contents should be involved to further optimize the composition of the alloys.

2. The preferential deformed and recrystallized textures were not observed in the present study, which can be a promising direction.

3. There was several sign in the present study showing that hot-rolling further promoted the precipitation of Mn-containing dispersoids, which can be discussed in the following study.

4. There is still a large body of heat treatment procedures can be applied, for instance 2-step heat treatment to further optimize the distribution of Mn-containing dispersoids, or an aging process after the post-deformation annealing to combine the strengthening effect of dispersoids and precipitates.

5. Observation performed on precipitation behavior of Mn-containing dispersoids and Zr, (Sc)-induced dispersoids were not completely matched on terms of heat treatment parameters. Therefore, a more detailed observation on Zr, Sc-induced dispersoids can be very promising to further clarify their interactions.